Copy
RM L57D26

RESEARCH MEMORANDUM

CHARACTERISTICS OF THE NIKE-CAJUN (CAN) ROCKET SYSTEM AND FLIGHT INVESTIGATION OF ITS PERFORMANCE

By John F. Royall, Jr., and Benjamine J. Garland

Langley Aeronautical Laboratory
Langley Field, Va.

NATIONAL ADVISORY COMMITTEE
FOR AERONAUTICS

WASHINGTON

July 29, 1957

NATIONAL ADVISORY COMMITTEE FOR AERONAUTICS

RESEARCH MEMORANDUM

CHARACTERISTICS OF THE NIKE-CAJUN (CAN) ROCKET SYSTEM AND FLIGHT INVESTIGATION OF ITS PERFORMANCE

By John F. Royall, Jr., and Benjamine J. Garland

SUMMARY

A Nike-Cajun (CAN) two-stage solid-propellant rocket vehicle was flight tested for performance. This rocket was a modification of the Nike-Deacon (DAN) rocket which had previously been flight tested to evaluate its use as a meteorological sounding rocket. The altitude capabilities of the system were determined by flight-test measurements which recorded a peak altitude of 426,000 feet when the vehicle was launched from sea level at an angle of 75°. Satisfactory performance of the CAN sounding rocket was indicated from the results of the flight test conducted.

A second Nike-Cajun combination known as the "hurricane rocket" was also flight tested. The only differences between this rocket and the University of Michigan Nike-Cajun sounding rocket were the weight, research apparatus, and the nose cone. This performance also proved to be satisfactory.

Sufficient additional information has been included to enable a prospective user to determine the characteristics of the system under a wide variety of operating plans.

INTRODUCTION

The Langley Pilotless Aircraft Research Division of the National Advisory Committee for Aeronautics, in conjunction with the Engineering Research Institute of the University of Michigan, developed and flight tested the Nike-Cajun (CAN) meteorological sounding-rocket system. This system was a modification of the Nike-Deacon (DAN) sounding rocket system which contained upper atmosphere research apparatus (ref. 1) and which was also developed through joint efforts of NACA and the University of Michigan. The Deacon motor has been replaced by the Cajun rocket motor in order to extend the altitude capabilities of the system.

Although the initial use of the CAN system is to conduct density measuring experiments such as those conducted with the DAN (ref. 1), it is also slated for use by various agencies for a number of different tasks. One of these is the photographing of hurricanes from high altitudes. This project was initiated by the U. S. Weather Bureau and is being conducted by the Office of Naval Research, Washington, D. C. and the Physical Science Laboratory, New Mexico College of Agricultural and Mechanical Arts. In order to check out this system, the NACA has flight tested the CAN system, equipped with the necessary photographic and recovery instrumentation. The nose section housing the equipment is considerably larger and heavier than the University of Michigan system; this difference resulted in reduced performance.

This report presents the configurations, flight-test results, and preflight calculations. The flight-test results are presented in the form of data for trajectories, velocities, accelerations, and drag. These data are valuable for determining the ability of the Nike-Cajun rocket to fulfill the needs of any particular high-altitude research mission. The detailed preflight information is presented to enable prospective users of this rocket system to analyze its abilities in terms of their own proposed flight conditions.

Flight tests were conducted at the Langley Pilotless Aircraft Research Station at Wallops Island, Va.

SYMBOLS

A	area, sq ft
A_F	frontal area, sq ft
a_X	longitudinal acceleration, ft/sec^2
C_D	drag coefficient, D/qA_F
C_{L_α}	lift-curve slope per radian
x_{cp}	center of pressure, in.
c_f	skin-friction coefficient
c_p	specific heat of air at constant pressure, $Btu/(slug)(^oF)$; specific heat of wall material or inner shield, $Btu/(lb)(^oF)$
D	drag, lb

g	acceleration due to gravity at altitude, $g_o \frac{r^2}{(r + h')^2}$, ft/sec^2
g_o	acceleration at sea level due to gravity, 32.174 ft/sec^2
h'	altitude, ft
h	local aerodynamic heat-transfer coefficient, Btu/(sec)(sq ft)(^oF)
M	Mach number
N_{St}	Stanton number, $\frac{h}{c_{p,l}\rho_l V_l}$
N_{Pr}	Prandtl number
q	dynamic pressure, lb/sq ft
q_{flt}	heating rate during flight, Btu/(sq ft)(sec)
Q	total heat, Btu/sq ft
Q_{flt}	total heat during flight, Btu/sq ft
r	radius of the earth, 20,898,609.60 ft
N_{Re}	Reynolds number per foot of length, $\frac{\rho V}{\mu}$
T	temperature, ^oR
t	time, sec
V	velocity, fps
R	horizontal range, ft
ϵ	emissivity
ρ	density of air, slugs/cu ft; density of wall material, lb/cu ft
σ	Stefan-Boltzmann constant, 4.835×10^{-13} Btu/(sq ft)(sec)(^oR)^4
τ	thickness of wall material, ft

Subscripts:

aw	adiabatic wall

s inner shield

t stagnation

l just outside the boundary layer or local

w skin or wall

DESCRIPTION OF THE VEHICLES

The Nike-Cajun (CAN) sounding rocket employed a two-stage solid-propellant propulsion system consisting of a first-stage Nike booster and a second-stage Cajun rocket motor. The use of the Cajun rocket motor in place of the ABL Deacon rocket motor represents the major difference between the CAN and the DAN rockets (ref. 1). A photograph of the Nike-Cajun (CAN) sounding rocket as used by the University of Michigan is shown on the launcher in figure 1. The first-stage Nike booster consisted of three parts: an adapter and coupling at the head end of the booster rocket, the rocket motor, and a fin assembly. The booster fin assembly (see fig. 2) consisted of four magnesium fins each welded to a magnesium quadrant. The four quadrants were held together by four longitudinal rods. The quadrants are in turn held to the booster motor by an aluminum shell which is attached to the motor and quadrants by screws. The second-stage Cajun sounding rocket consisted of three major components: the instrument-housing nose section, the Cajun rocket motor, and the fin assembly. The nose cone contained an AN/DPN-19 radar beacon and an accelerometer sphere. During the flight the nose cone ejected from the model and the sphere released by means of a spring. The Cajun fin assembly (see fig. 3) consisted of four extruded sections, each section consisting of an aluminum fin and a quarter section of the shroud. The four sections were held together with longitudinal pins and were attached to the motor by means of a threaded ring located inside the assembled quadrants. A $\frac{1}{32}$-inch-thick Inconel cap covered the leading edge of each of the second-stage Cajun fins to protect them against aerodynamic heating.

The construction of the Nike-Cajun (CAN) rocket used for hurricane tests (herein called the hurricane rocket) is the same as the University of Michigan Nike-Cajun (CAN) sounding rocket except for the nose section. Photographs of the hurricane rocket are presented in figures 4 and 5.

Sketches of the CAN system as flight tested for the University of Michigan and the hurricane project are shown in figure 6. The differences between the two systems are the nose sections. The weights of the various components are presented in the following table:

Loaded booster, lb	1,170.00
Booster adapter, lb	27.00
Booster fins, lb	76.50
Complete booster, lb	1,273.50
Loaded Cajun, lb	166.90
Cajun fins, shroud, and fairing ring, lb	30.00
Nozzle extension, lb	5.00
Nose cone and instrumentation (sounding rocket), lb	51.85
Nose cone and instrumentation (hurricane rocket), lb	75.77
Complete Cajun second stage (sounding rocket), lb	253.75
Complete Cajun second stage (hurricane rocket), lb	277.67

GROUND INSTRUMENTATION

The NACA modified SCR-584 tracking radar unit tracked a signal from an AN/DPN-19 radar beacon housed within the nose cone of the University of Michigan sounding rocket and provided slant range, azimuth, and elevation angle from which altitude, horizontal range, and flight-path angle may be calculated at a given time. No beacon was carried in the hurricane rocket and consequently it was skin tracked by the radar unit for only a portion of its flight. A rawinsonde, employing a balloon that was launched before the time of flight, provided measurements of static pressure, static temperature, and balloon azimuth and elevation to altitudes in excess of 60,000 feet. Wind velocity and direction were calculated from these data.

The CW Doppler radar unit measured the variation of velocity with time during the early portion of the flight. The velocities thus obtained were then used with values of the speed of sound in order to obtain Mach number. The speed of sound was calculated from static-temperature measurements obtained from the rawinsonde.

TEST RESULTS

The CAN system as used by the University of Michigan was launched at an angle of elevation of 75° from horizontal. The second stage was boosted to an altitude of 5,000 feet. The booster then separated from the second stage since the deceleration of the burned-out booster was greater than that of the second-stage motor. The second stage coasted 8.9 seconds before the Cajun sustainer rocket fired and was accelerated to a maximum velocity of 6,250 feet per second at an altitude of 40,000 feet. After burnout, the second stage coasted in free flight, gaining altitude. The nose cone and sphere were released 52 seconds after launching took place. A peak altitude of 426,000 feet was determined

from the AN/DPN-19 radar beacon in the nose cone at 170 seconds after ground launching. The nose cone was tracked to splash at a range of 472,000 feet and time of 343 seconds.

Results of the hurricane rocket as compared with the University of Michigan sounding rocket are presented in figures 7 to 11. Figure 7 shows trajectory plots of the two rockets, figure 8 represents the variation of altitude with flight time for both flight tests, figure 9 shows the variation of velocity and Mach number with time for both rockets, figure 10 presents the variation of Reynolds number per foot of length with Mach number, and figure 11 shows a plot of longitudinal acceleration with time. It should be pointed out that the acceleration obtained from the NACA modified SCR-584 radar is less accurate than that obtained from the CW Doppler radar.

Trajectory plots of the Nike-Cajun (CAN) sounding rocket and the Nike-Deacon (DAN) sounding rocket are presented in figure 12 to illustrate the effect of changing from the Nike-Deacon (DAN) to the Nike-Cajun (CAN).

The variation of drag coefficients with Mach number for the first coast period of the second stage is presented in figure 13.

PREFLIGHT CALCULATIONS

Drag

The calculated drag coefficients are presented in figures 13, 14, and 15 with figure 13 also showing the total measured drag coefficients for both CAN systems. The values of the drag coefficients of the CAN combination when thrusting are presented in figure 14. Changes in the nose shape of the two models appear to have little effect on the total drag coefficient. Figure 13 presents the breakdown of the drag coefficient of the second-stage rocket when coasting. The major difference between the drag of the University of Michigan sounding rocket and the drag of the hurricane rocket is the size of the nose cone. When the rocket is thrusting there will be a decrease in the drag caused by the base. The increase of drag due to adding caps to the leading edge of the fins is shown. The reason for adding these caps will be discussed in the section on aerodynamic heating. It should be noted that the step drag (step shown on model sketch in fig. 6) is simply conical pressure drag over its annular area and is a very rough calculation. The total drag will depend on the flight conditions which influence the skin friction. Typical values of the skin-friction coefficient of the hurricane and sounding rockets are presented in figure 15 for different flight

conditions. The differences between the skin friction of the two configurations are small. The method of reference 2 was used to obtain values of the skin friction by assuming that the entire boundary layer was turbulent.

Aerodynamic-Heating Considerations

The performance capabilities of the CAN (M = 6) make it subject to severe aerodynamic-heating conditions. The successful flight-test results presented herein indicate that the design was adequate to withstand the heating encountered. The sequent sections will discuss how these heating conditions influenced the design and also the temperatures that the various components are estimated to have reached during the flight. The methods used in estimating the temperatures herein may be applied to other trajectories and heating conditions that the CAN system may be exposed to. The assumptions as to the local flow conditions used in calculating the temperatures of the various components were purposely kept simple. Experience has indicated that these estimates are sufficiently accurate for design calculations and in general are conservative. An example is the neglect of the effect of the blunting of the nose tip on the flow conditions over the rest of the conical nose. Particular attention should be paid to the aerodynamic heating when the CAN system is used at higher Mach numbers and lower altitudes. Figure 16 presents the preflight estimated variation of Mach number and altitude with time for the University of Michigan sounding rocket which was used for the following calculations.

Nose heating.- Knowledge of the temperature rise of the nose skin during the flight is important for two reasons: to insure structural integrity of the model and to determine if radiation of heat from the skin is sufficient to affect the instruments carried within.

The skin temperatures estimated for the University of Michigan CAN nose are presented in figure 17. These temperatures were calculated by using a heat-balance equation as follows:

$$\rho_w c_{p,w} \tau_w \frac{dT_w}{dt} = h(T_{aw} - T_w) - \text{Radiation} - \text{Conduction} \qquad (1)$$

where h is the local aerodynamic heat-transfer coefficient and equal to $N_{St}\rho_l V_l C_{p,l}$ and

$$T_{aw} = N_{Pr}^{1/3}(T_t - T_l) + T_l \qquad (2)$$

By using the known properties of the material, local conditions on the conical nose (subscript l) and theoretical Stanton number N_{St} as given

by the turbulent theory of Van Driest (ref. 2) and modified for use with a cone (ref. 3) and neglecting conduction terms, the temperatures may be calculated by using a step-by-step procedure. These calculations were based on preflight estimates of model performance (fig. 16). The flight results were close enough to estimated conditions that it was not considered necessary to recalculate for measured flight conditions.

The calculated temperatures are well within the accepted range for Inconel and no difficulty would be expected from load considerations.

By using these values of wall temperature, the temperature reached by a cylindrical inner shield may be estimated with the following equation which was obtained from the material in reference 4.

$$\rho_s \tau_s c_{p,s} \frac{dT_s}{dt} = \frac{\sigma A_w \left(T_w^4 - T_s^4 \right)}{A_s \left[\frac{A_w}{A_s} \left(\frac{1}{\epsilon_s} \right) + \frac{1}{\epsilon_w} - 1 \right]} \tag{3}$$

where the subscript s refers to the inner shield and the subscript w refers to the cone skin or wall. It would be more correct to calculate the inner shield and outer shield temperatures simultaneously since the heat radiated to the inner shield reduces the wall or skin temperature T_w. Equation (3) is adequate for a first approximation, however.

Additional heat may be transferred from the skin to inner parts of the model through various structural paths. This may be minimized by putting insulating materials such as Micarta in the heat paths between the outer skin and the inner structure.

The comments so far have been concerned with temperatures on the cone surface generally. The heat-transfer rate at the nose tip will be considerably higher. For this reason the nose tip has been blunted (0.151 in. radius) and a large heat sink has been created by making the nose solid steel for several inches back. A discussion of heat transfer to spherical tips is given in reference 5.

Cajun case heating.- During firing of the Cajun sustainer motor the average internal operating pressure of the motor is 1,080 psi. It is therefore necessary to insure that the case is not heated externally to a temperature where the strength of aluminum has been materially reduced.

Temperatures therefore have been calculated on the case near the fore end, where the maximum aerodynamic heating should occur. The calculations were similiar to those used for the nose heating with several exceptions. The local conditions (subscript l) used were those for the nose cone. These values will give an upper limit and therefore conservative values of local aerodynamic heat-transfer coefficient h. It is

felt that the calculation of local conditions at the fore end of the cylinder by such sophisticated methods as "characteristics" was not warranted. The results of the temperature calculation are given in figure 17. A temperature of 730° R is reached while the motor is burning, and a maximum temperature of 910° R is reached 11.1 seconds after burnout due to heat added by aerodynamic heating. The heat added due to the motor burning will be negligible. Neither of these temperatures is excessive for the respective loading conditions.

If the CAN system were used at very low altitudes where motor case temperatures were calculated to be excessive, a "quick fix" in the form of spirally wrapping the motor with glass tape may be used. A more elaborate solution would take the form of a thin metal shell over the case, which would take only friction loads. The motor case would remain as primary structure. Both of these methods have been used satisfactorily by the Langley Pilotless Aircraft Research Division for high Mach number, low-altitude conditions.

Fin heating.- The fin assembly was constructed of aluminum as described previously and is shown in figure 3. The temperatures on the fin surface 2 inches from the leading edge were estimated by using the heat balance equation as before. Free-stream conditions were assumed, thereby treating the fin as a flat plate. The thickness term τ is assumed to be one-half the fin thickness since heat is being transferred to both sides. The temperatures calculated at two spanwise stations with thicknesses of 0.10 inch and 0.20 inch are presented in figure 18. The melting temperature and the temperature at which aluminum has dropped to one-half its room temperature strength are also indicated. It is seen that the fin reaches a temperature higher than the half-strength temperature. This occurs at a time of about 6 seconds for the 0.1-inch-thick station and occurs again for the 0.1-inch-thick and 0.2-inch-thick stations at a time well after maximum Mach number and at considerable altitude where the loads are considerably lower than maximum design conditions. This condition should be noted in varying the trajectory of the CAN system.

The design of a fin leading edge for high-speed flight is very difficult because the local heating rates are extremely high and because accurate calculations of these rates are difficult. For example, the maximum heating rate to the bare basic aluminum fin leading edge is about 20 times that to the fin surface 2 inches back from the leading edge. The calculation of the fin leading-edge temperature is complicated by the fact that conduction effects, that is, the heat being diffused into the heavier fin structure behind the leading edge, cannot be neglected. Because of this difficulty in estimating leading-edge temperatures, experimental methods were used to evaluate the leading-edge design. Tests were conducted in the ethylene jet which is a blowdown jet which operates at a Mach number of 2 with a ram-jet burner located upstream

of the nozzle. Ethylene is introduced and burned in the stream and in this way the stagnation temperature may be increased as high as 4,000° R. A more complete description of this facility is presented in reference 6. The jet was used in the following manner to simulate the flight-test conditions. The quantity of heat q being transferred to the leading edge at any time during the flight is equal to

$$q_{flt} = h(T_{aw} - T_w)$$

$$q_{flt} = N_{St}\rho V c_p(T_{aw} - T_w)$$

or the total heat transferred would equal

$$Q_{flt} = \sum_{t=0}^{t=i} N_{St}\rho V c_p(T_{aw} - T_w)\Delta t$$

At any given time, however, T_w is not known because part of the heat is being conducted away. However, an upper limit of Q can be calculated by assuming that T_w remains constant at preflight air temperatures. On the other hand, a minimum Q may be calculated by assuming no conduction. (In this case the heat capacity (volume) of the leading edge was assumed to be that of a half-cylinder or radius equal to that of the leading edge.) With these upper and lower values of Q_{flt}, tunnel stagnation temperature and running time were varied to give the same q values. The basic aluminum fin was tested under these conditions. The fin was observed (cameras and timing clock) to begin burning at 1.7 seconds; this indicates this fin might not be satisfactory in flight. As a result the leading edges of the fins were modified in order to insure the fin against failure or damage due to aerodynamic heating. Results presented in reference 6 have shown that a simple practical way of improving the heating characteristics of the leading edges of lightweight material fins consists of capping the forward several inches of the fin with 0.032-inch Inconel. The Inconel capping gives the benefits of the high-melting-point characteristics of that metal in the area where it is needed without the penalizing effect of constructing the entire fin out of Inconel. Whether the fin were made from a solid piece of Inconel or fabricated from sheet, large penalties would be paid in weight (performance) or in simplicity of design and construction.

A second fin with Inconel capped leading edge has been tested in the ethylene jet. The fin, exposed to the same stagnation temperatures as the uncapped fin, lasted 2.2 seconds or more than 30 percent longer. These results indicate the capped fin would withstand satisfactorily the heating through the maximum Mach number condition. The satisfactory flight-test results confirm the conservatism of the simulation procedure.

STABILITY

In the stability calculations for the University of Michigan sounding and the hurricane rockets, the values of C_{L_α} and x_{cp} for the cylinder were taken from data gathered in reference 7. It should be noted that at a Mach number of 4 the values of C_{L_α} and x_{cp} were assumed to reach their maximum and that above Mach number 4 the values were estimated.

The values of C_{L_α} for the fins up to a Mach number of 2 were calculated by using unpublished material from the Langley Pilotless Aircraft Research Division. The values above a Mach number of 2 were calculated by the method of reference 8.

For the nose cone the values of x_{cp} were assumed to be two-thirds back from the nose tip and the values of C_{L_α} were taken from reference 9.

Figure 19 shows a comparison of the centers of pressure as a function of Mach number for the University of Michigan sounding and hurricane rockets. The only difference between the two models is the nose shape. It is shown that the difference in center of pressure for the Cajun sustainer rocket alone, for the two CAN systems with these different nose shapes varied between 6 and 8 inches, whereas the center of pressure for the Nike-Cajun combination was the same. With these values of center of pressure and center of gravity (also shown in fig. 19) the University of Michigan sounding and the hurricane rockets appeared to have adequate static stability. This information should prove to be useful for other Nike-Cajun systems with different nose shapes.

A variation of the product of lift-curve slope times area with Mach number for the Cajun cylinder and fins and a variation of center of pressure with Mach number for the Cajun cylinder are presented in figure 20. The center of pressure for the fins is assumed to be at 50 percent of the mean aerodynamic chord which is at the 97.1-inch station. The center of pressure for the cylinder and fins is measured from the front of the cylinder.

Figure 21 presents a variation of the product of the lift-curve slope and the area and center of pressure with Mach number for the Nike booster. The Nike booster is divided into its three components: the adapter, cylinder, and fins, and the values of $C_{L_\alpha}A$ are presented as such. Values of C_{L_α} for the adapter were calculated by the equation

$$C_{L_\alpha} = \left(C_{L_\alpha}\right)_{cone}\left[\left(\frac{D_2}{D_1}\right)^2 - 1\right]$$

where D_1 = 7.1 inches and is the diameter of the front of the adapter and D_2 = 17.5 inches and is the diameter of the rear of the adapter. This makes the appropriate reference area $\frac{\pi D_1^2}{4}$. These values are presented so that the center-of-pressure calculations of other Nike-Cajun combinations may be made easily by substituting into the following equation:

$$x_{cp,comb} = \frac{\Sigma\left(x_{cp}C_{L_\alpha}A\right)_{Nike} + \Sigma\left(x_{cp}C_{L_\alpha}A\right)_{Cajun\ components}}{\Sigma\left(C_{L_\alpha}A\right)_{Nike} + \Sigma\left(C_{L_\alpha}A\right)_{Cajun\ components}}$$

Performance

The calculated effects of loaded second-stage weight, drag, coast time, and launching angle on the trajectory of the Nike-Cajun system for the hurricane rocket are presented in figures 22, 23, and 24. The effect of the loaded second-stage weight and drag on the maximum altitude is presented in figure 22. The time between burnout of the Nike and the firing of the Cajun (coast time) was 15 seconds and the launching angle was 90°. The effect of adding the leading-edge caps and subsequent increase in drag on the maximum altitude was small. This figure also presents the values of the drag coefficients which were used to calculate the trajectories. These drag values are not the same as those presented in figures 14 and 15 but the difference would affect the trajectories only slightly.

The effect of the coast time on the maximum altitude and maximum range for a given second-stage weight and launching angle is presented in figure 23. Between 8 and 18 seconds the maximum altitude varies only 1 percent, whereas the maximum range increases by 18 percent. Therefore, the maximum range is probably of more importance than the maximum altitude in determining the coast time.

The effect of the launching angle on the calculated maximum altitude and maximum range is presented in figure 24. The launching angle has a large influence on both the maximum altitude and the maximum range. The launching angle for maximum altitude is 90°; whereas the launching angle for maximum range is approximately 60°. The launching angle for maximum altitude will always be 90° but the angle for maximum range will depend upon the loaded second-stage weight, coast time, and drag.

CONCLUDING REMARKS

The University of Michigan Nike-Cajun (CAN) sounding rocket and the Nike-Cajun (CAN) rocket used for hurricane tests were both successfully flight tested and the drag, trajectories, and some velocity and acceleration information were obtained. Comparison of the flight data and preflight calculations indicates that it is possible to calculate accurately the performance by using calculated drag information.

The effects of the loaded second-stage weight, drag, coast time, and launching angle on the calculated performance of the hurricane rocket were presented. These results indicated the general effect of the parameters on any Nike-Cajun system.

Usually the loaded second-stage weight and the drag are determined by the purpose for which the system is intended. Therefore, the coast time and the launching angle are the only parameters which are varied to obtain the desired performance. However, the effects of aerodynamic heat transfer and aerodynamic loads must be considered in the selection of the coast time and the launching angle.

Langley Aeronautical Laboratory,
National Advisory Committee for Aeronautics,
Langley Field, Va., April 12, 1957.

REFERENCES

1. Heitkotter, Robert H.: Flight Investigation of the Performance of a Two-Stage Solid-Propellant Nike-Deacon (DAN) Meteorological Sounding Rocket. NACA TN 3739, 1956.

2. Van Driest, E. R.: Turbulent Boundary Layer in Compressible Fluids. Jour. Aero. Sci., vol. 18, no. 3, Mar. 1951, pp. 145-160, 216.

3. Van Driest, E. R.: Turbulent Boundary Layer on a Cone in a Supersonic Flow at Zero Angle of Attack. Jour. Aero. Sci., vol. 19, no. 1, Jan. 1952, pp. 55-57, 72.

4. Schmidt, Ernst: Thermodynamics. The Clarendon Press (Oxford), 1949.

5. Goodwin, Glen: Heat-Transfer Characteristics of Blunt Two- and Three-Dimensional Bodies at Supersonic Speeds. NACA RM A55L13a, 1956.

6. Bland, William M., Jr., and Bressette, Walter E.: Some Effects of Heat Transfer at Mach Number 2.0 at Stagnation Temperatures Between 2,310° and 3,500° R on a Magnesium Fin With Several Leading-Edge Modifications. NACA RM L57C14, 1957.

7. Buford, W. E., and Shatunoff, S.: The Effects of Fineness Ratios and Mach Number on the Normal Force and Center of Pressure of Conical and Ogival Head Bodies. Memo. Rep. no. 760, Ballistic Res. Labs., Aberdeen Proving Ground, Feb. 1954.

8. Lawrence, H. R., and Flax, A. H.: Wing-Body Interference at Subsonic and Supersonic Speeds - Survey and New Developments. Jour. Aero. Sci., vol. 21, no. 5, May 1954, pp. 289-324.

9. Ames Research Staff: Equations, Tables, and Charts for Compressible Flow. NACA Rep. 1135, 1953. (Supersedes NACA TN 1428.)

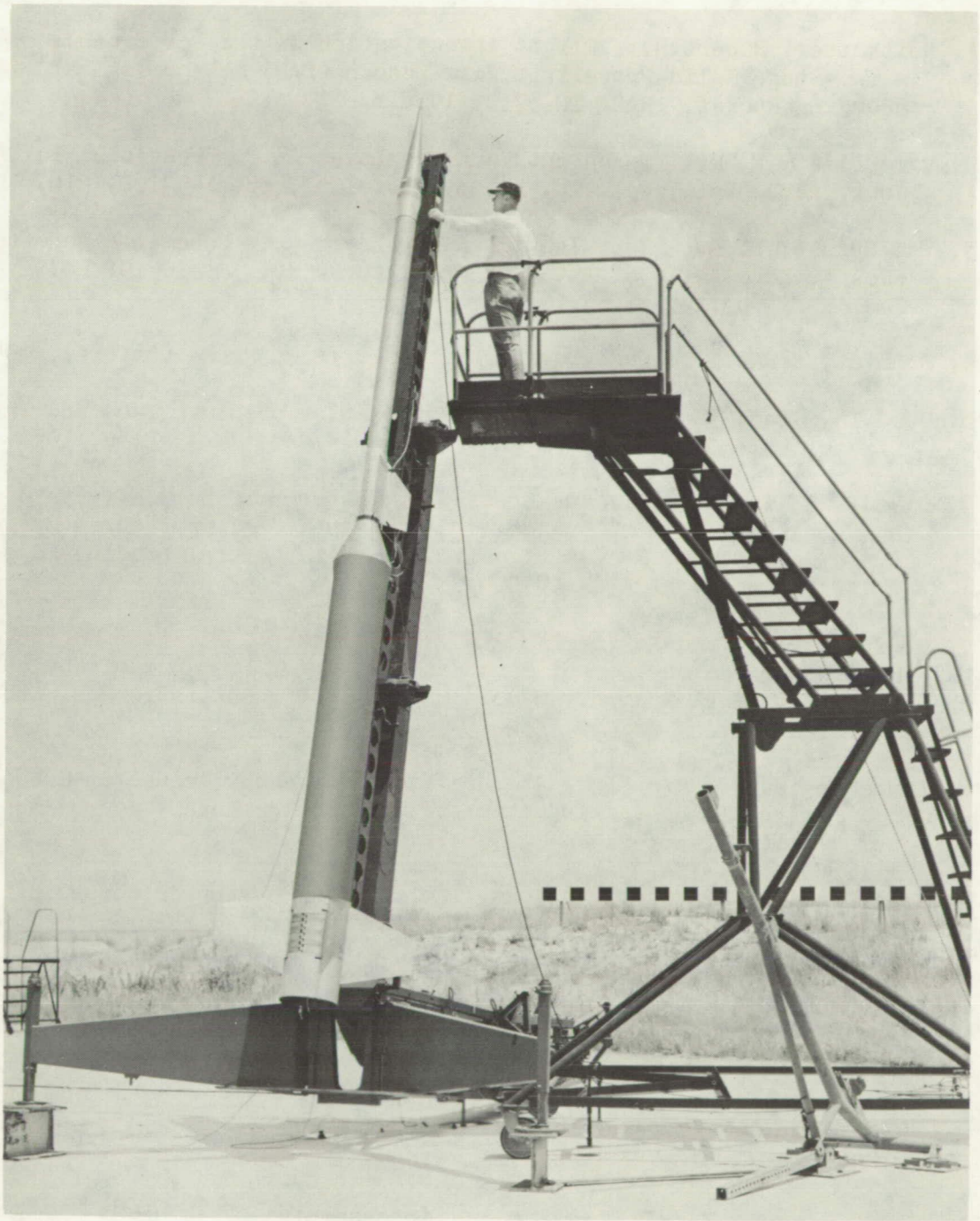

L-94722.1

Figure 1.- University of Michigan Cajun sounding rocket and the Nike booster on launcher.

Figure 2.- Booster fin assembly. L-97091.1

Figure 3.- Cajun fin assembly. L-97095

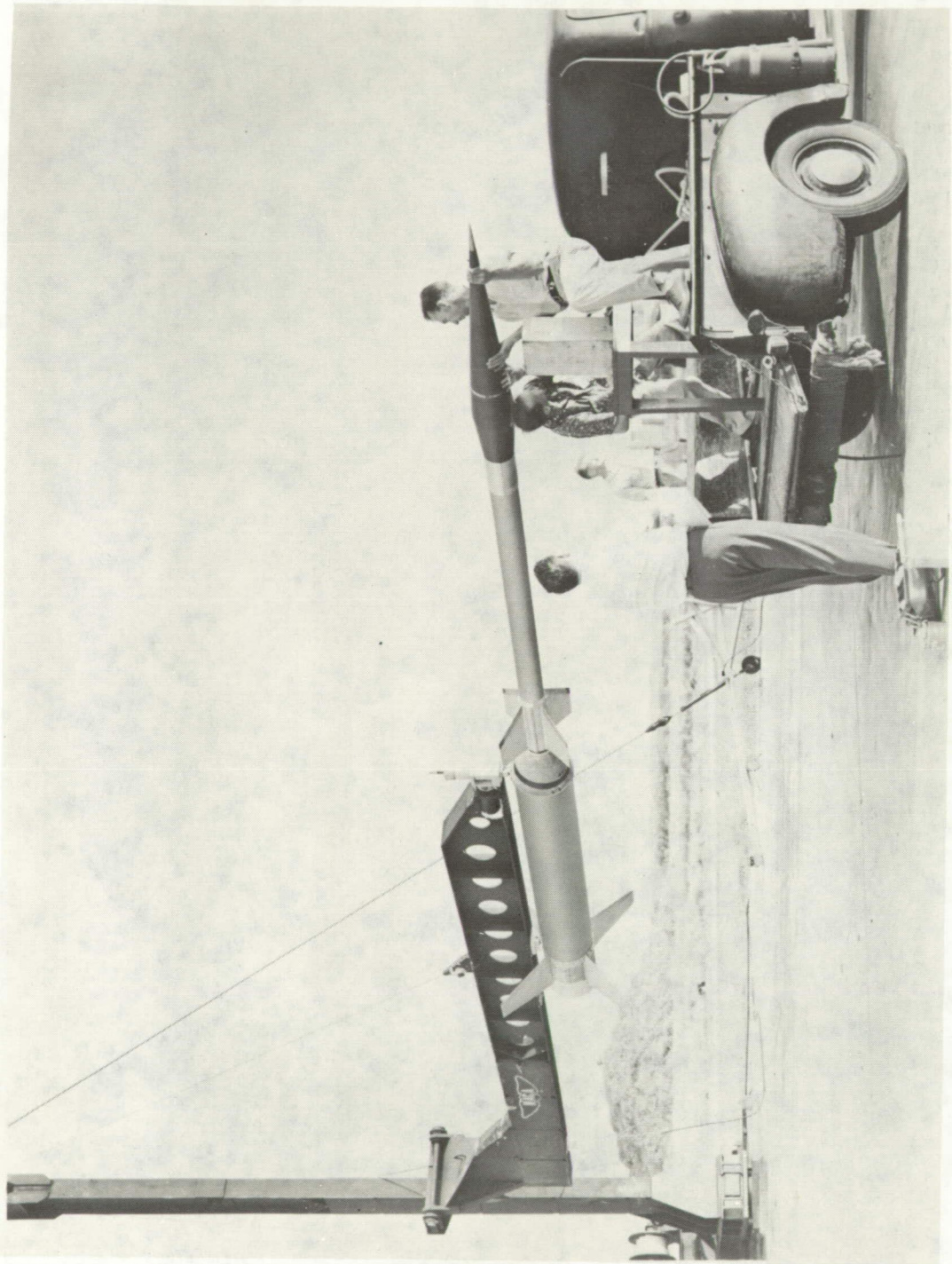

L-94860.1

Figure 4.- Hurricane Cajun rocket and Nike booster being assembled on launcher.

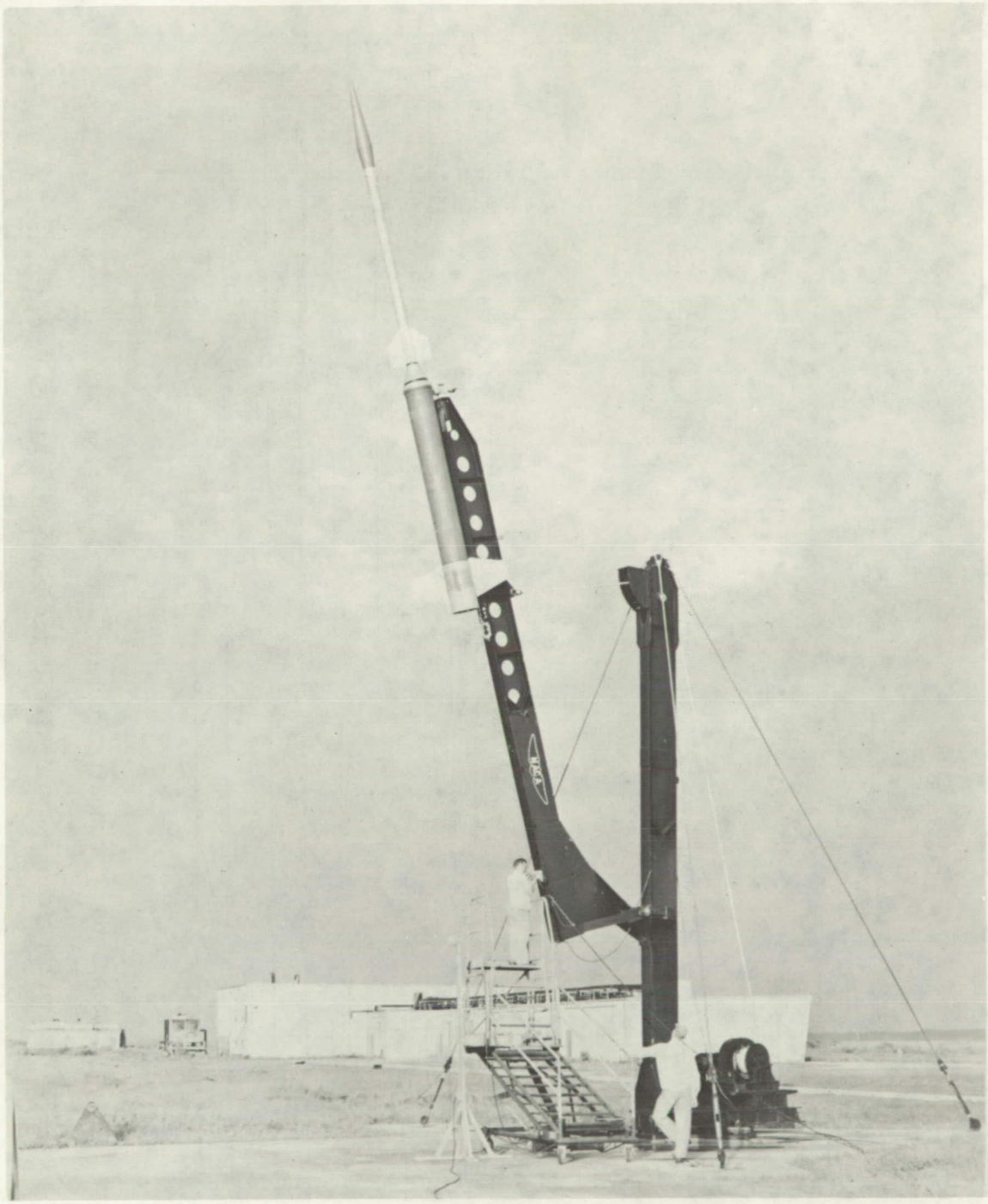

L-94862

Figure 5.- Hurricane Cajun rocket and Nike booster in firing position on launcher.

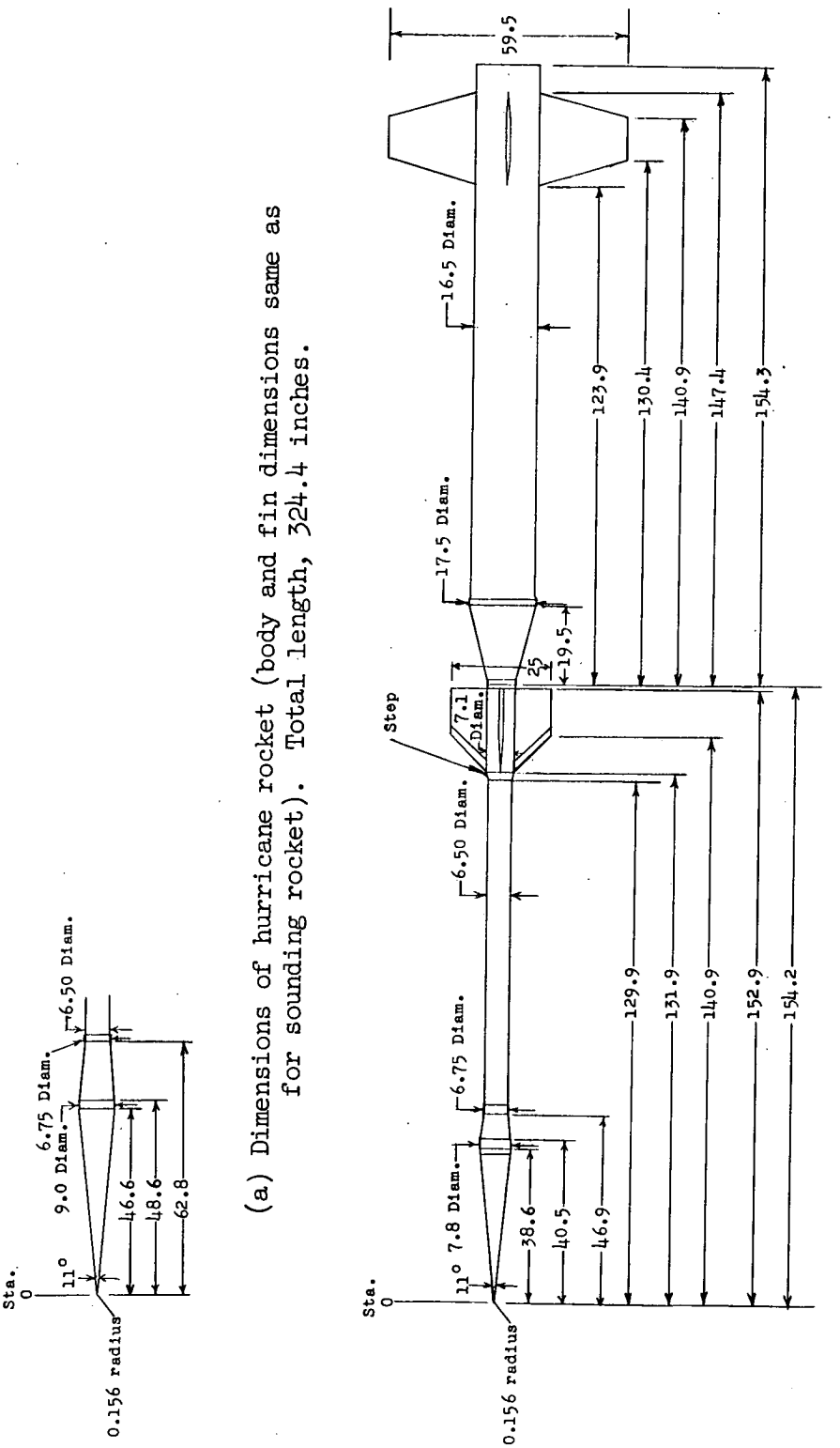

(a) Dimensions of hurricane rocket (body and fin dimensions same as for sounding rocket). Total length, 324.4 inches.

(b) Dimensions of sounding rocket. Total length, 308.5 inches.

Figure 6.- General arrangement of the Nike-Cajun rockets. All dimensions are in inches.

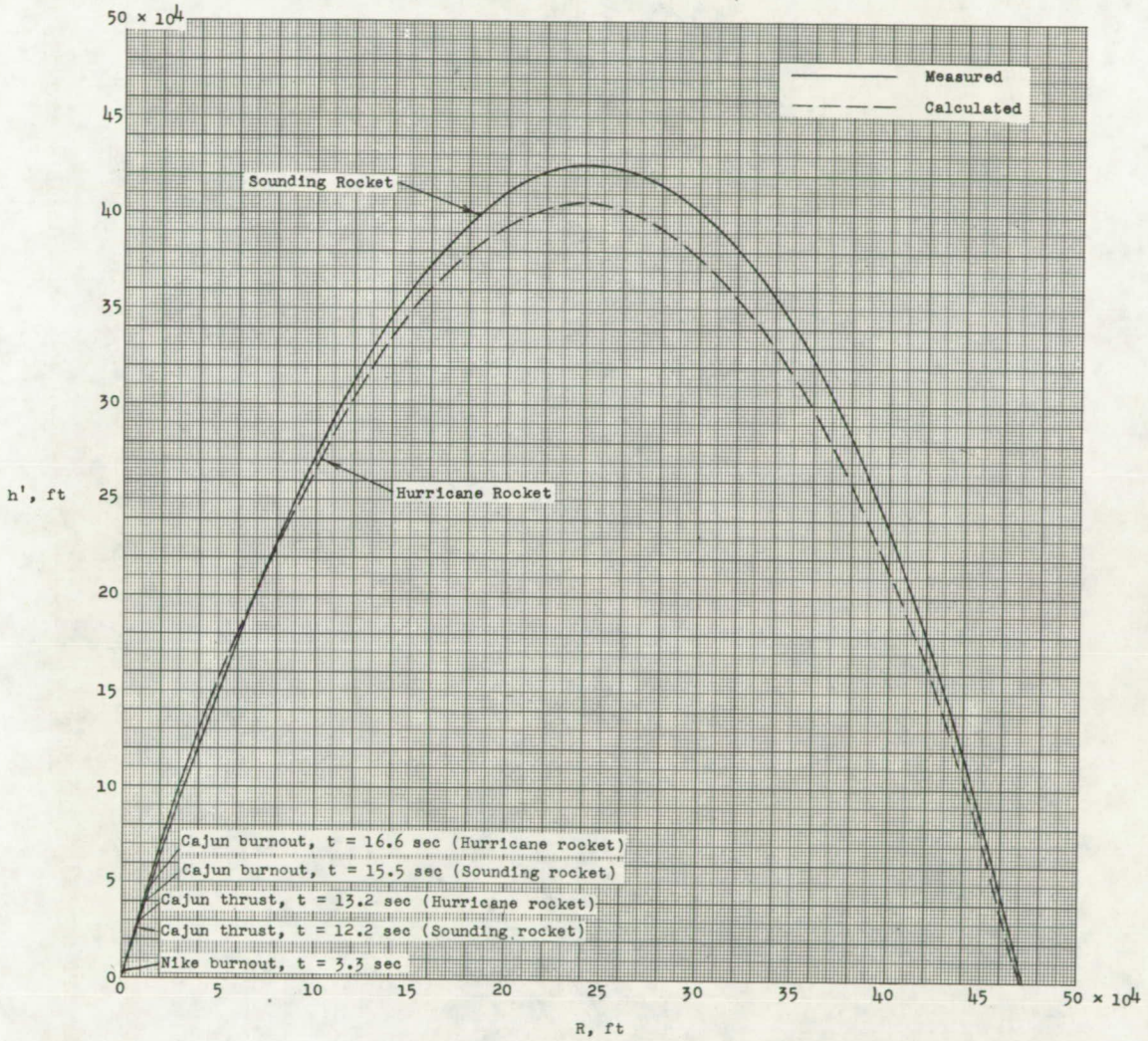

Figure 7.- Trajectories of the Nike-Cajun rockets.

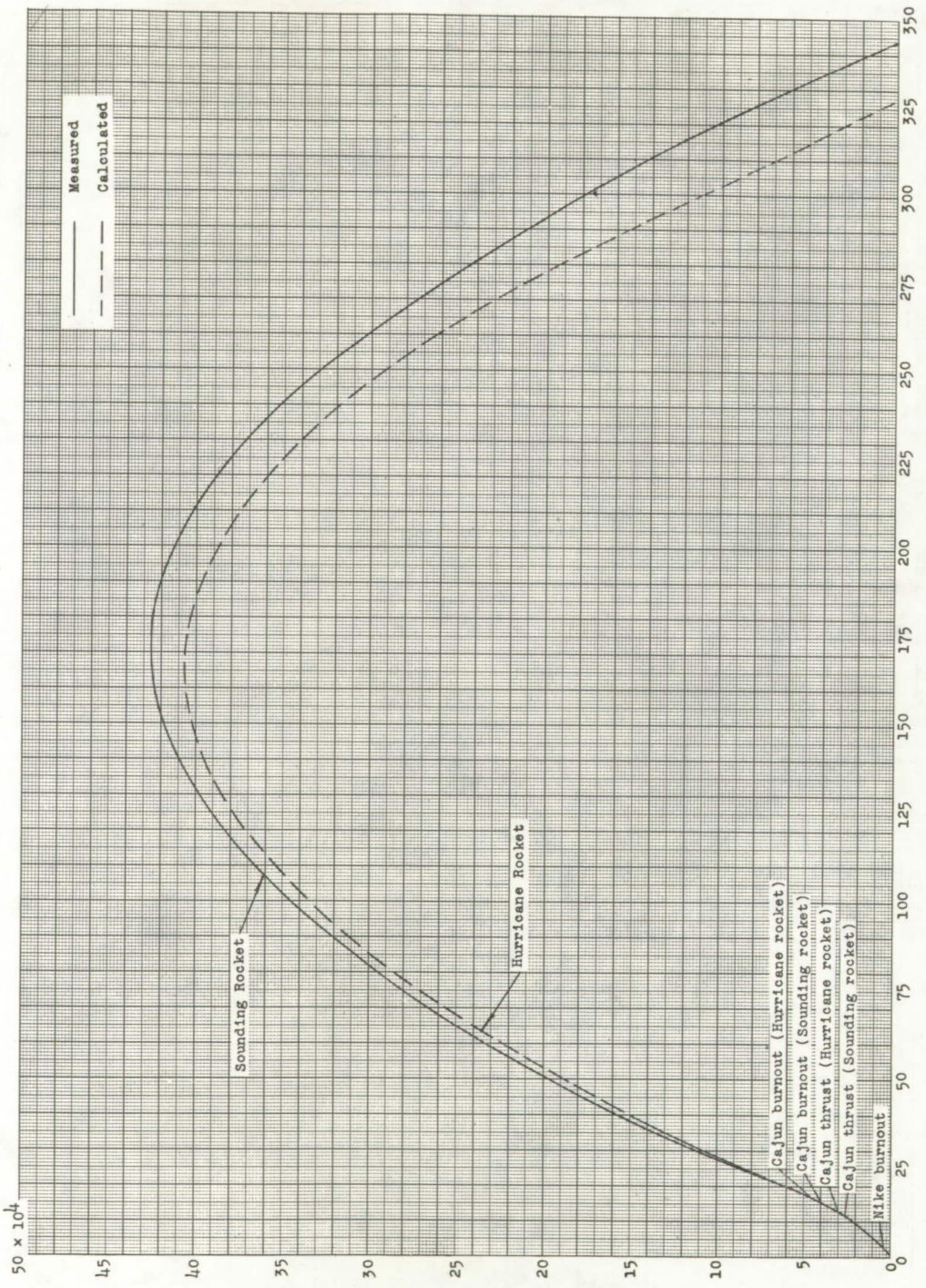

Figure 8.- Variation of altitude with time.

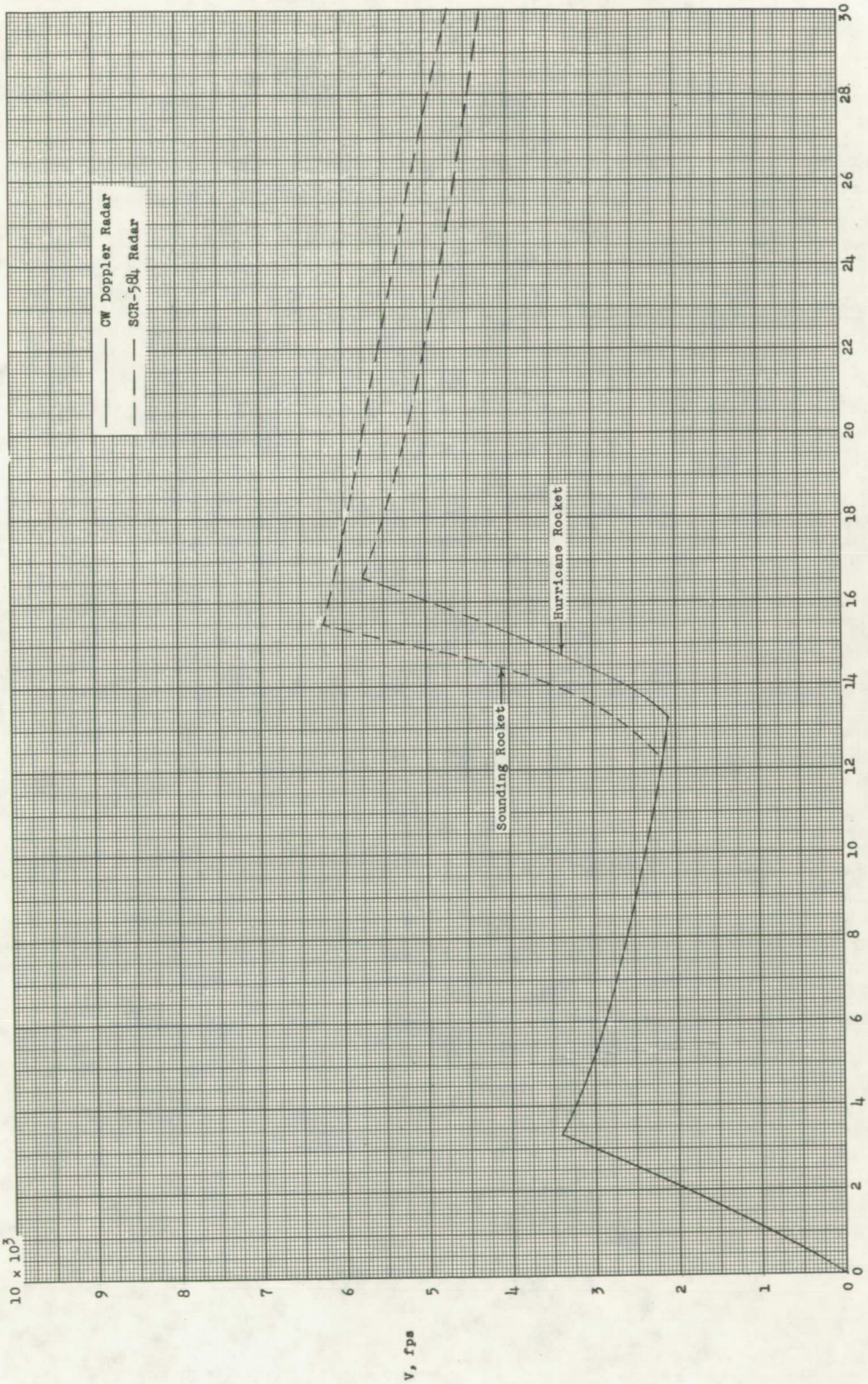

(a) Velocity.

Figure 9.- Variation of velocities and Mach number with time.

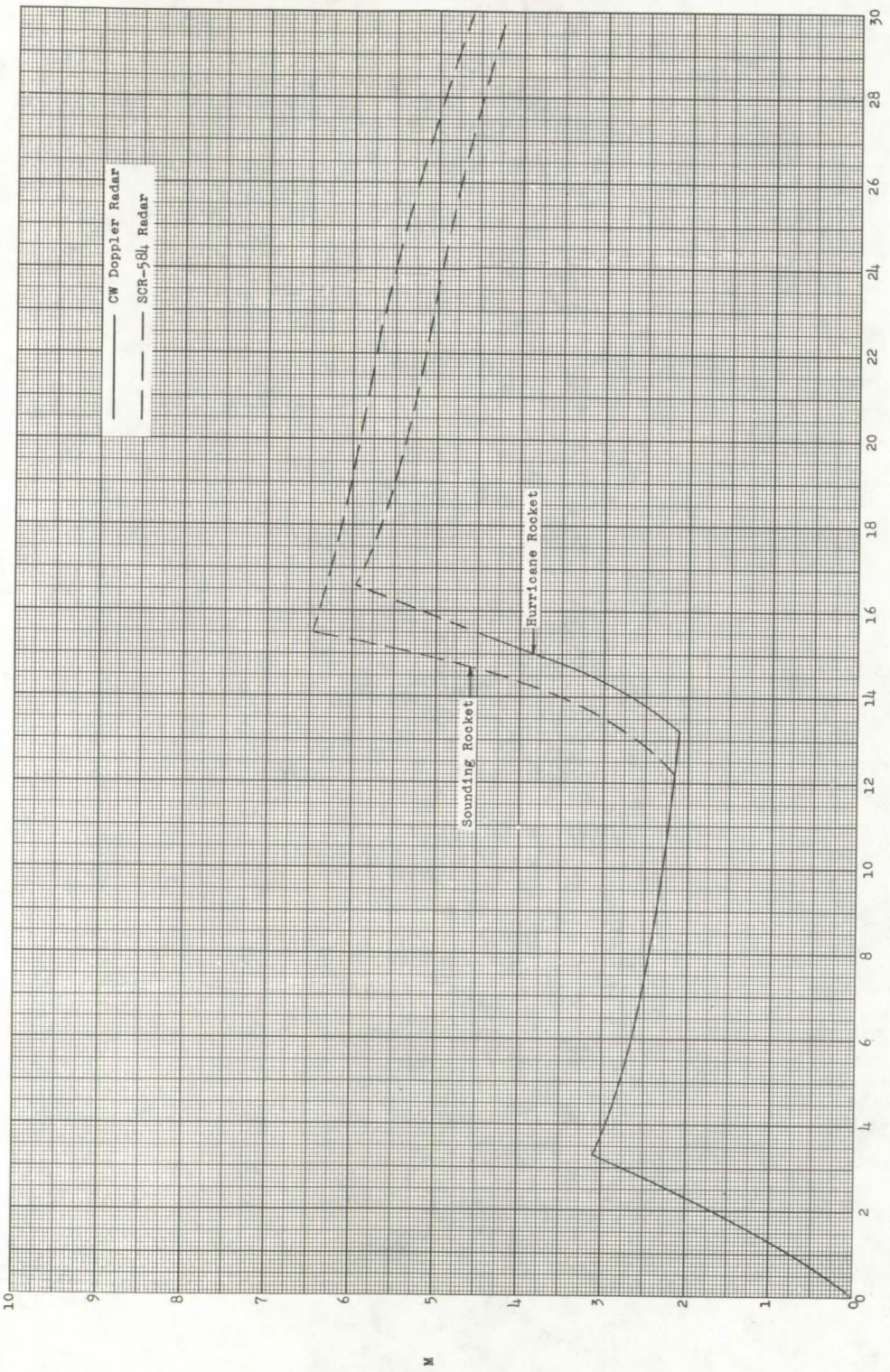

(b) Mach number.

Figure 9.- Concluded.

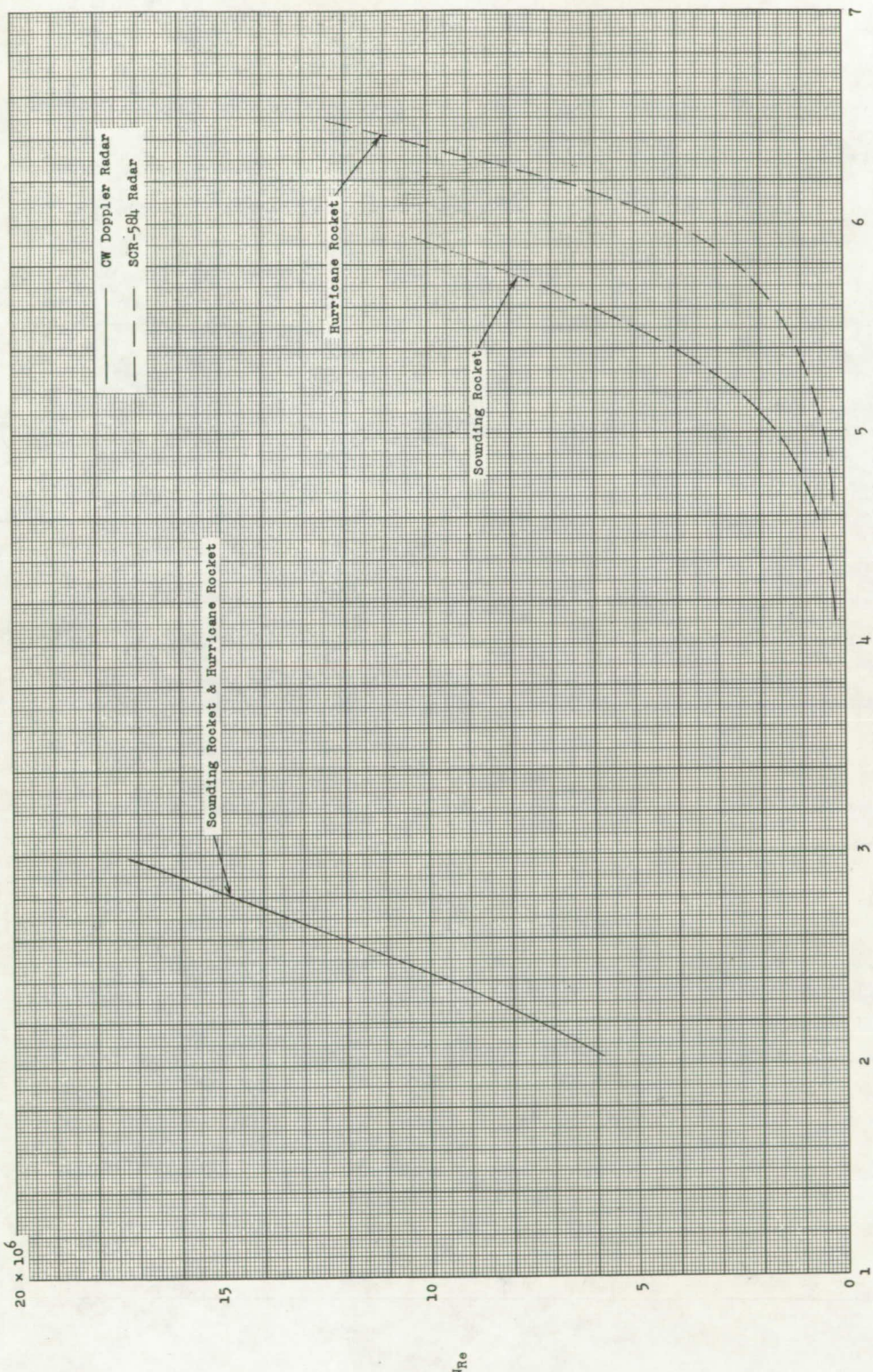

Figure 10.- Variation of Reynolds number per foot of length with Mach number.

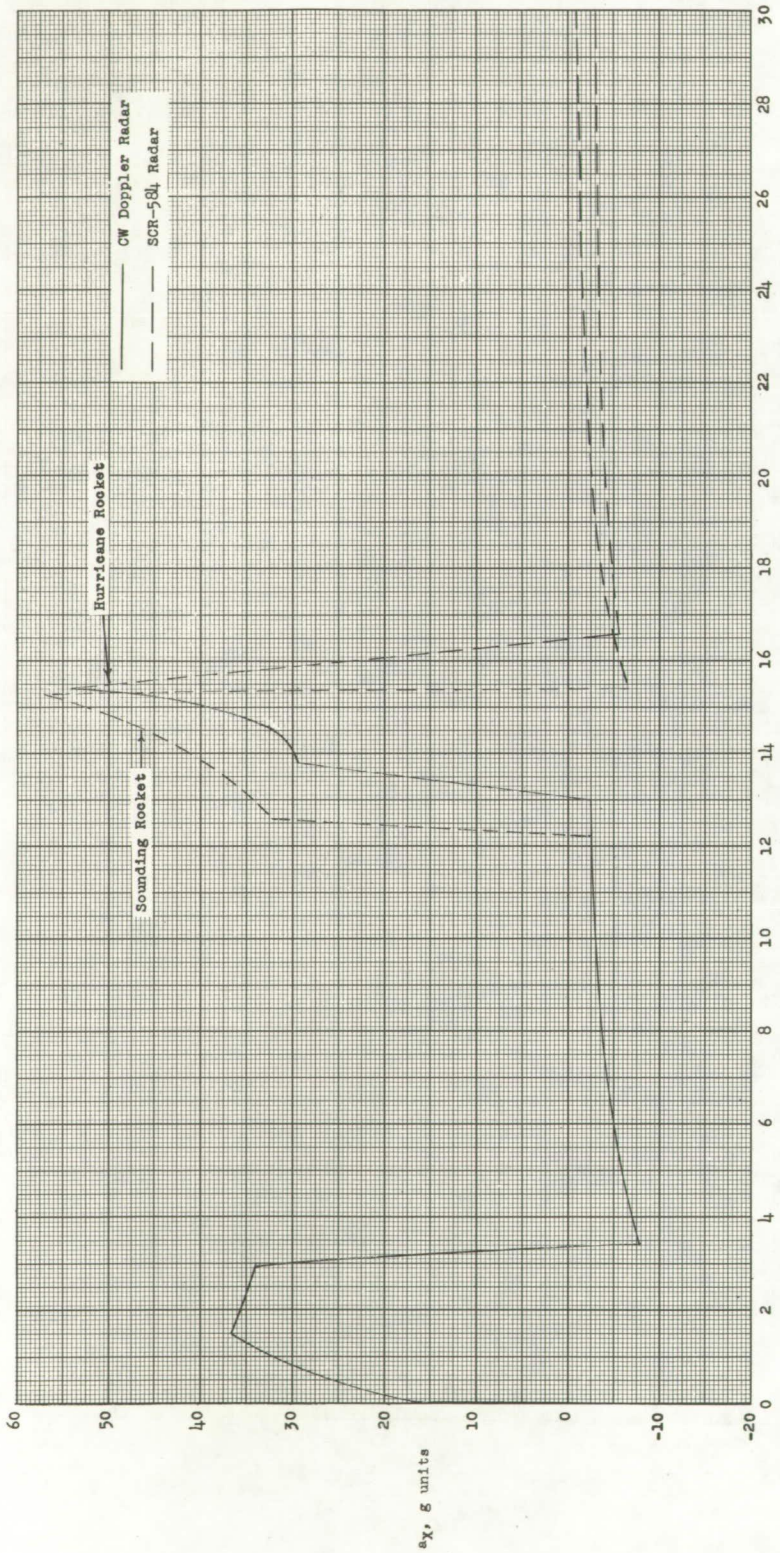

Figure 11.- Variation of longitudinal acceleration of the Nike-Cajun rockets with time.

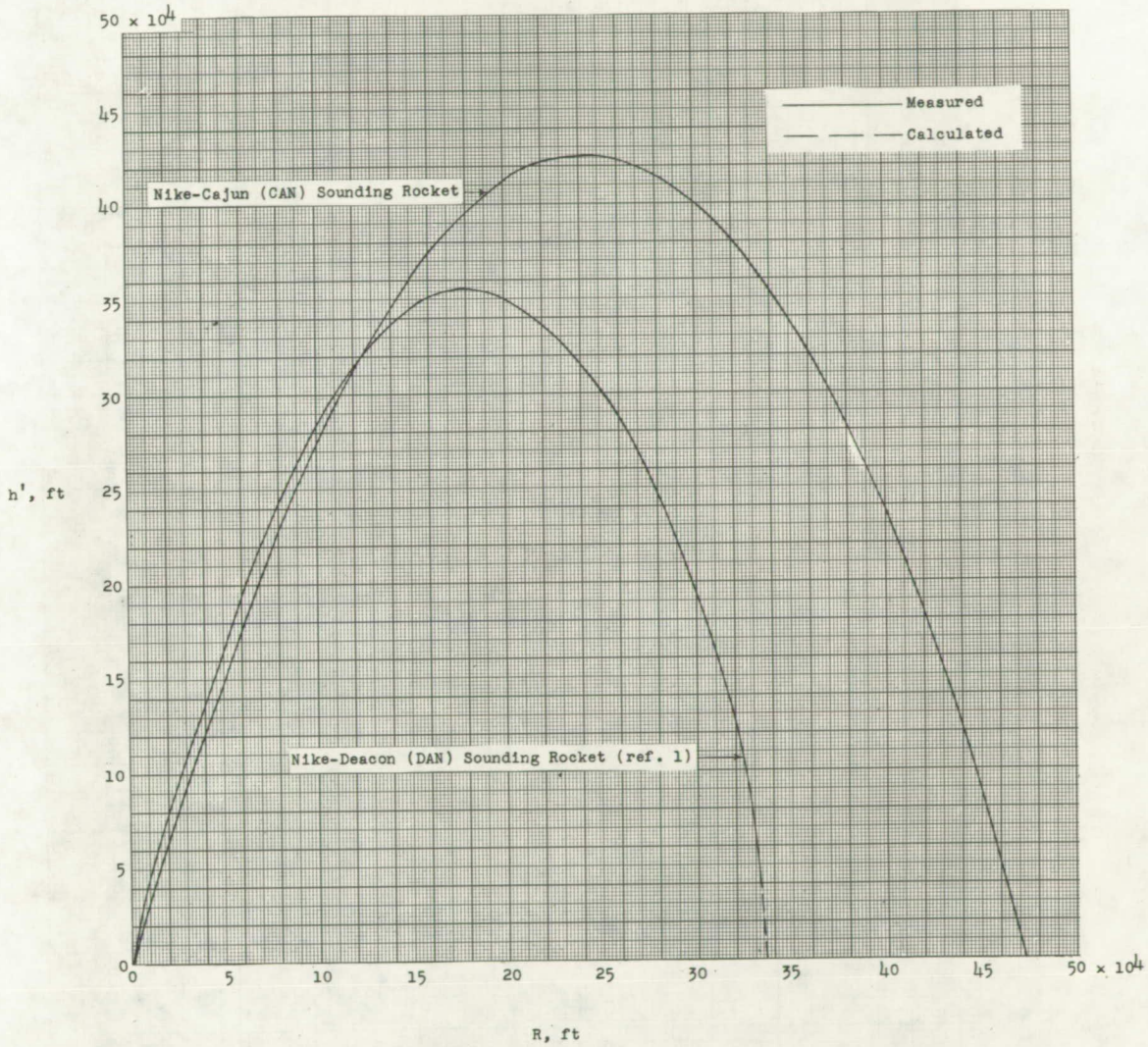

Figure 12.- A comparison of trajectories of University of Michigan Nike-Cajun (CAN) rocket and Nike-Deacon (DAN) rocket.

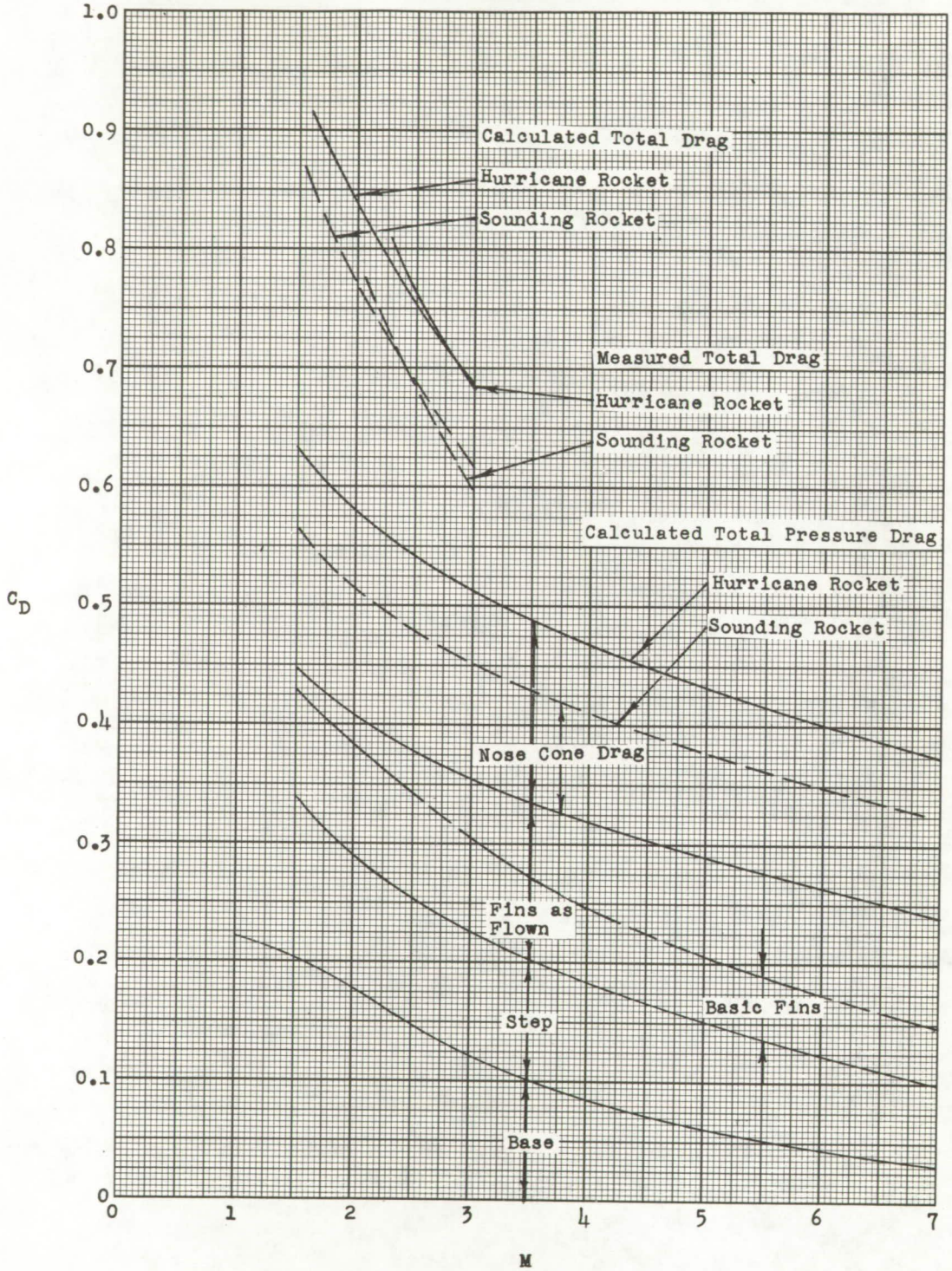

Figure 13.- Variation of drag coefficient with Mach number based on a diameter of 6.50 inches for Cajun coasting.

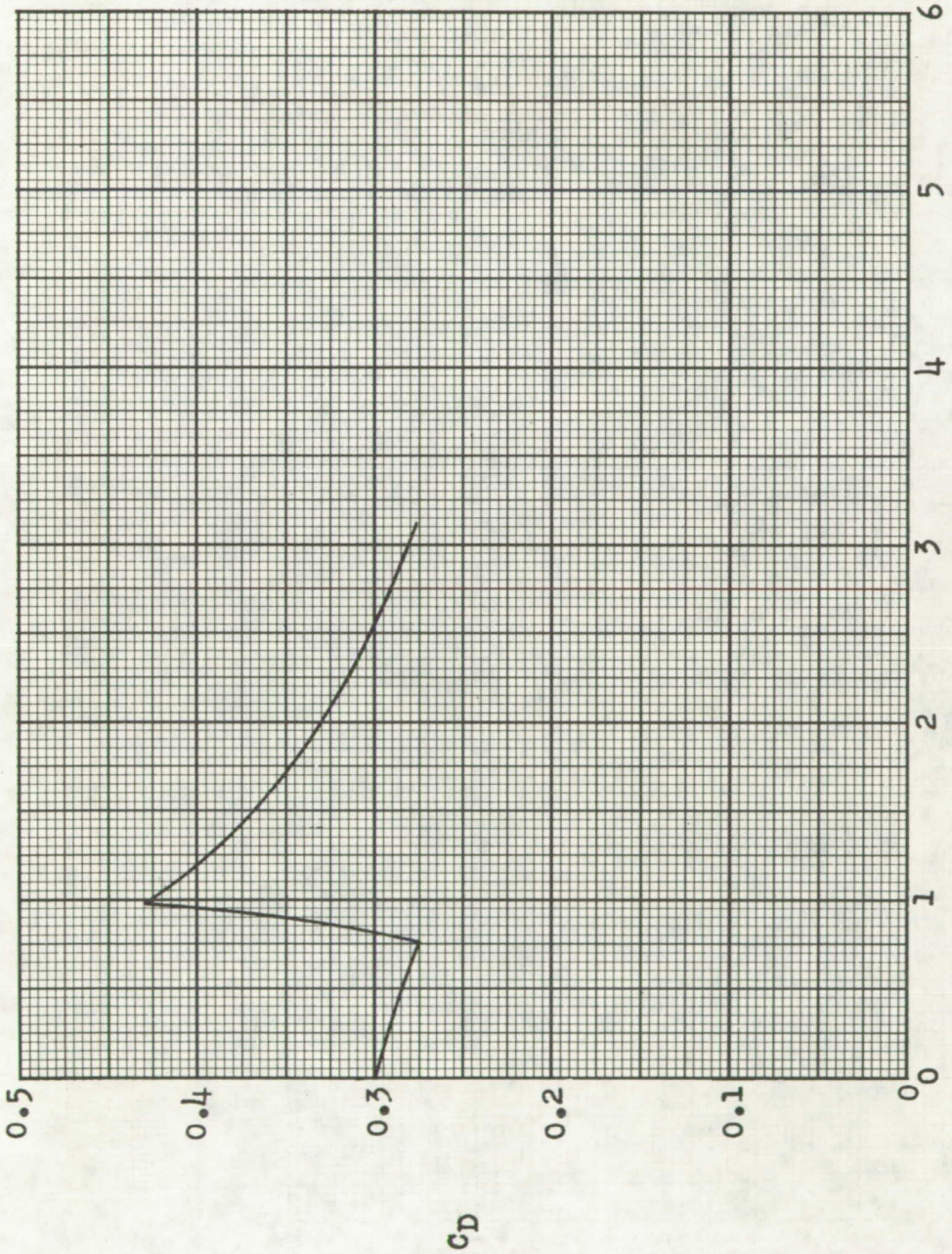

Figure 14.- Variation of calculated drag coefficient with Mach number based on a diameter of 16.5 inches for Nike-Cajun thrusting.

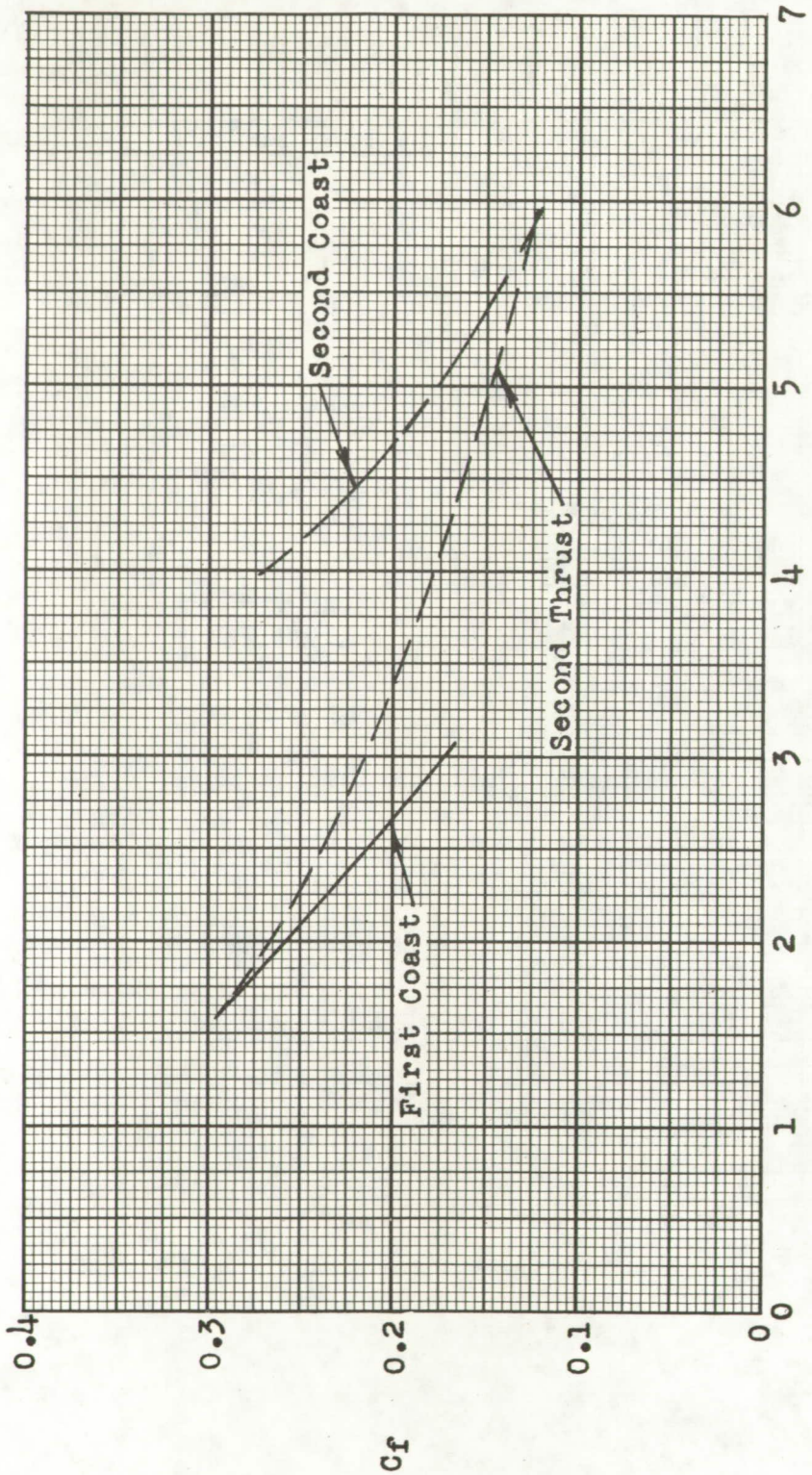

Figure 15.- Variation of calculated skin friction coefficient of second stage with Mach number based on a diameter of 6.50 inches for several flight conditions.

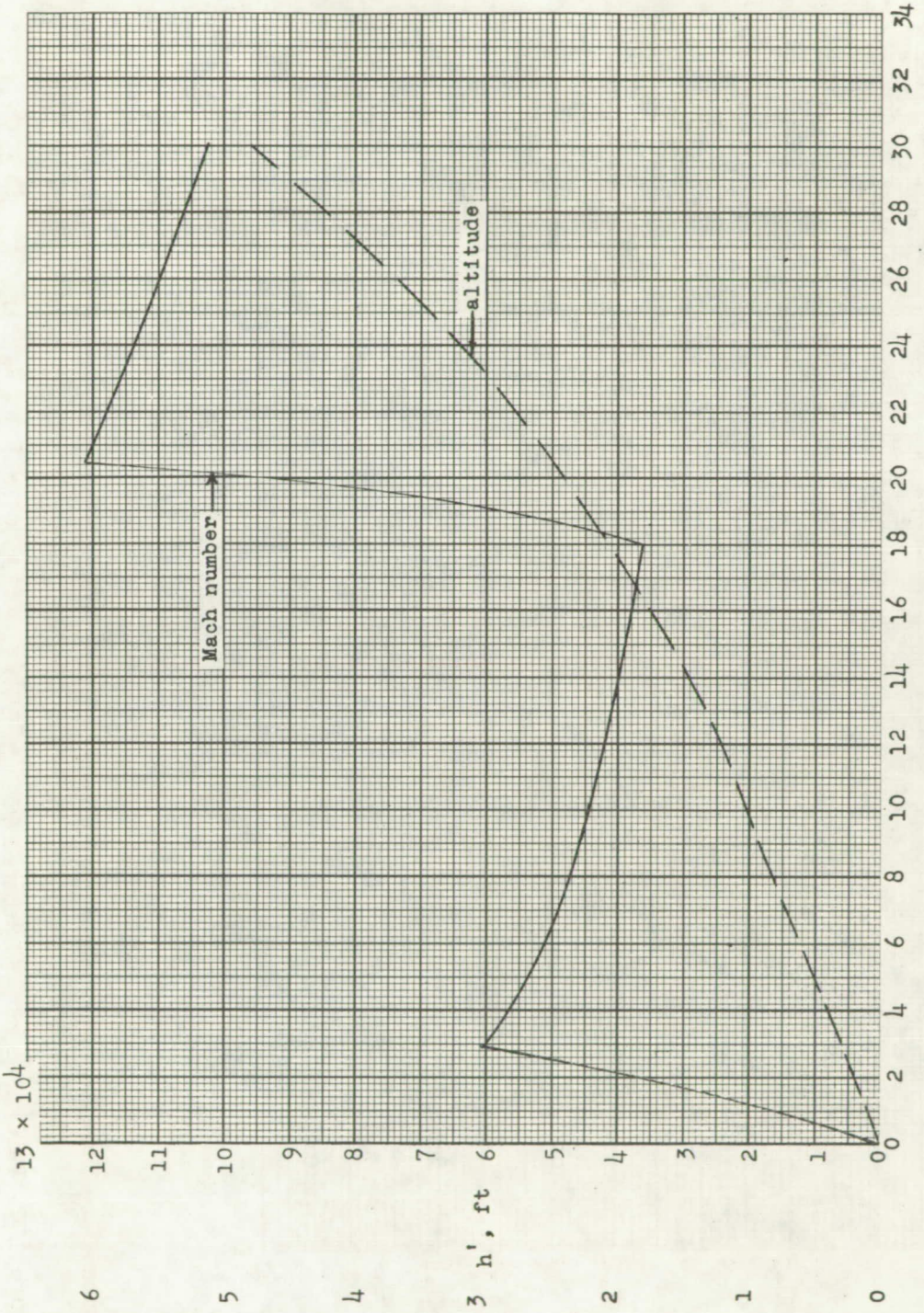

Figure 16.- Variation of calculated Mach number and altitude with time for University of Michigan Nike-Cajun sounding rocket.

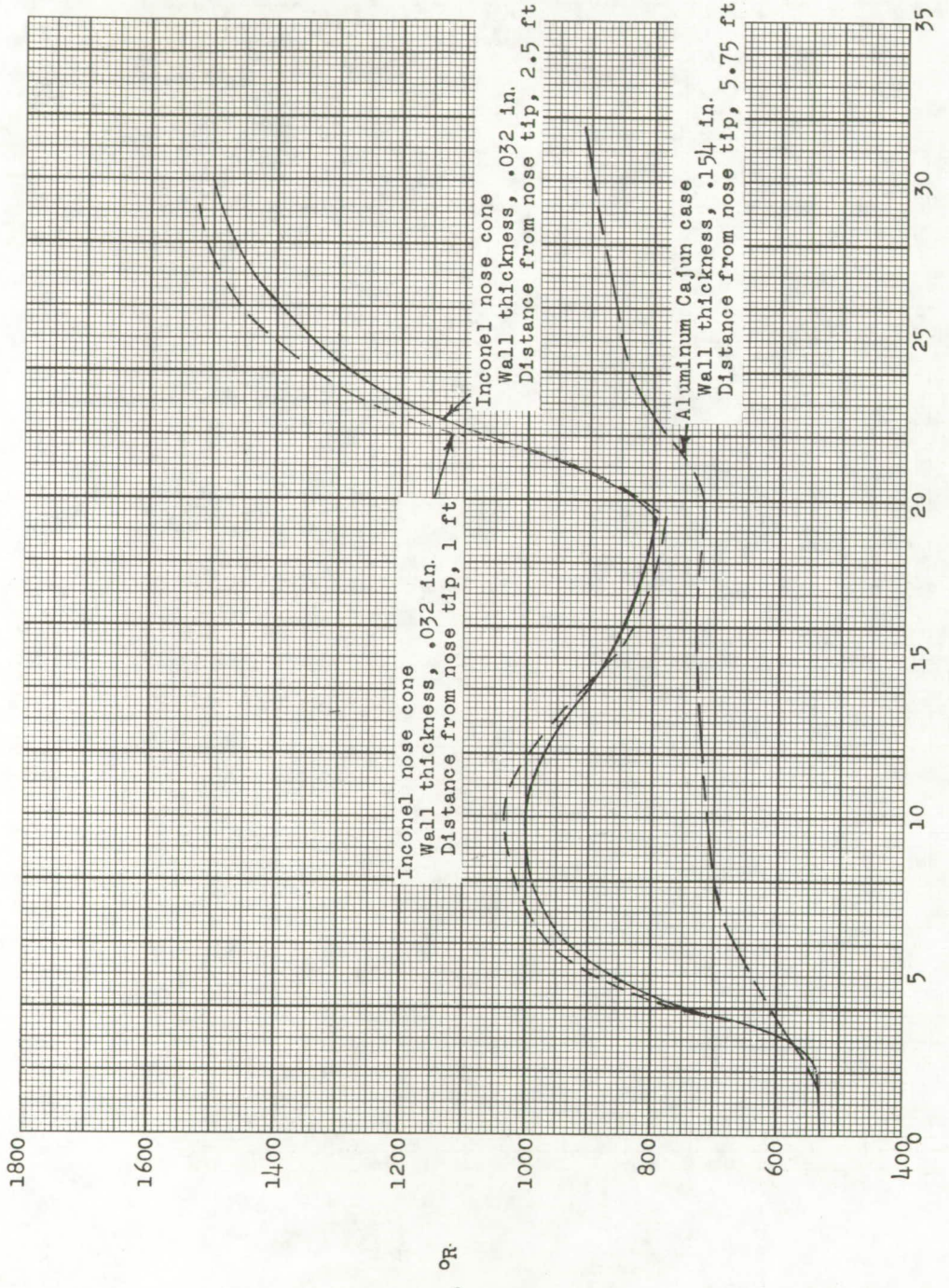

Figure 17.- Variation of calculated wall temperature with time for Inconel nose cone and aluminum Cajun case.

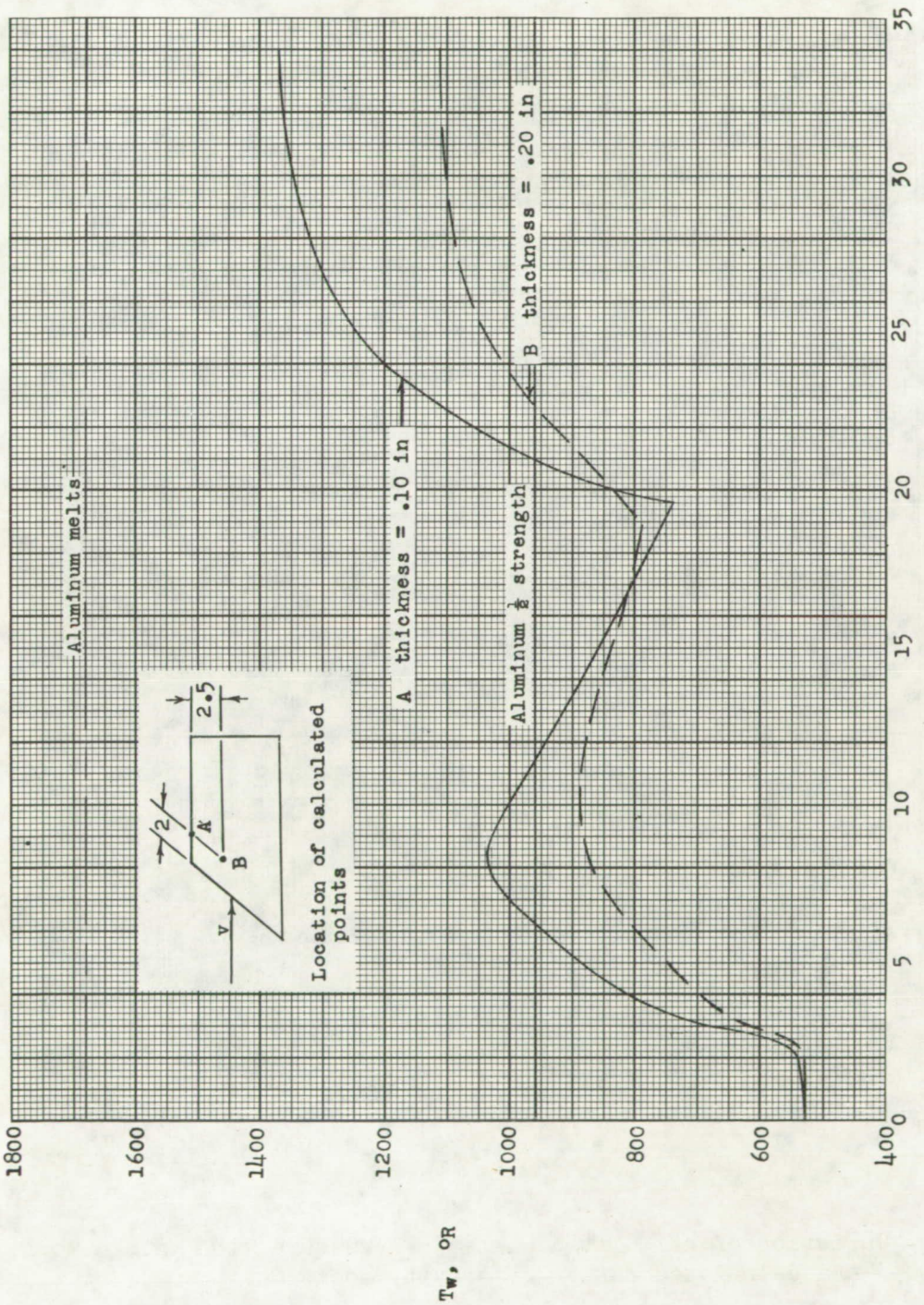

Figure 18.- Variation of calculated wall temperature with time for aluminum Cajun fin at a distance of 2 inches from the leading edge.

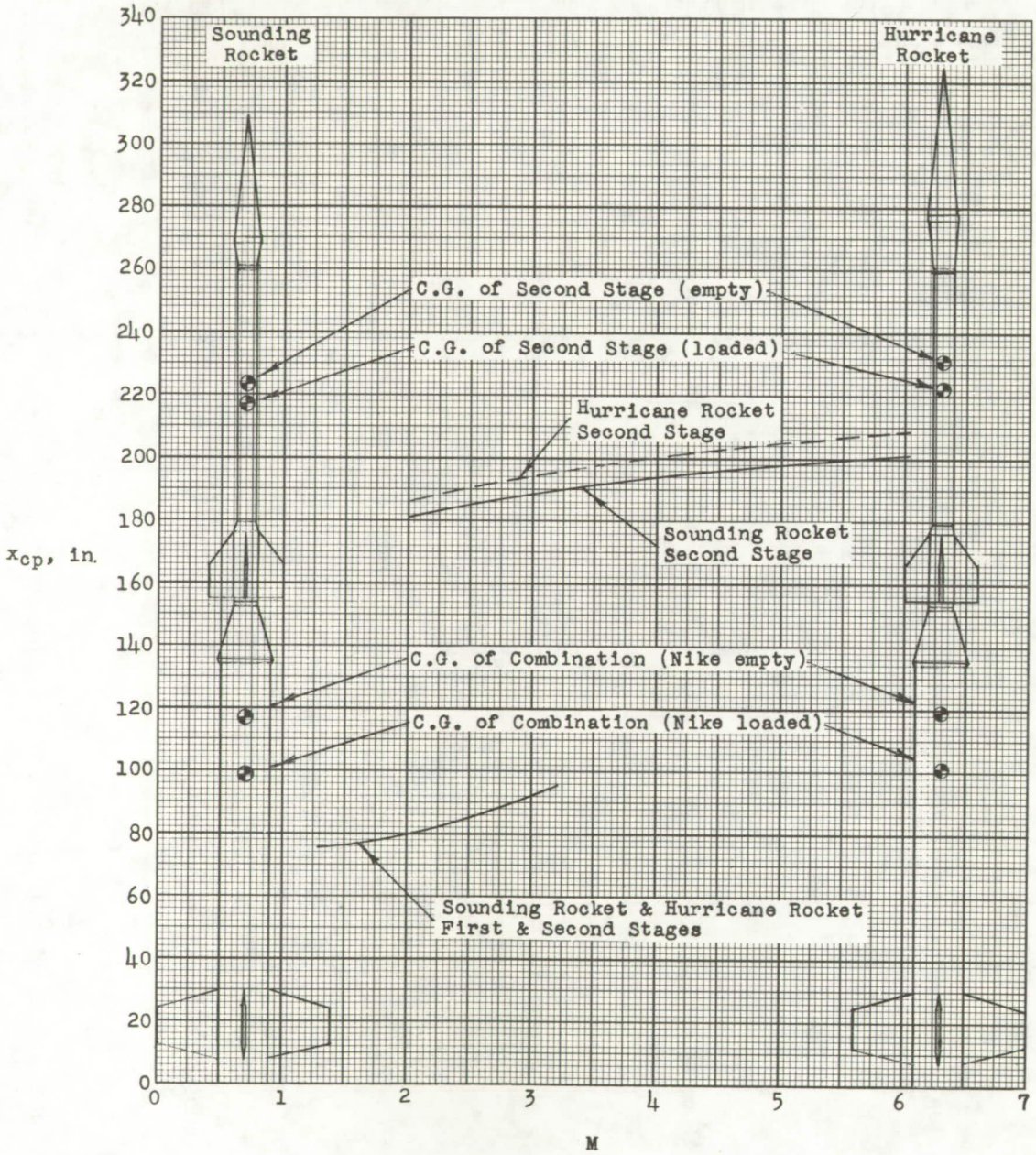

Figure 19.- Variation of calculated center of pressure with Mach number and calculated center-of-gravity locations.

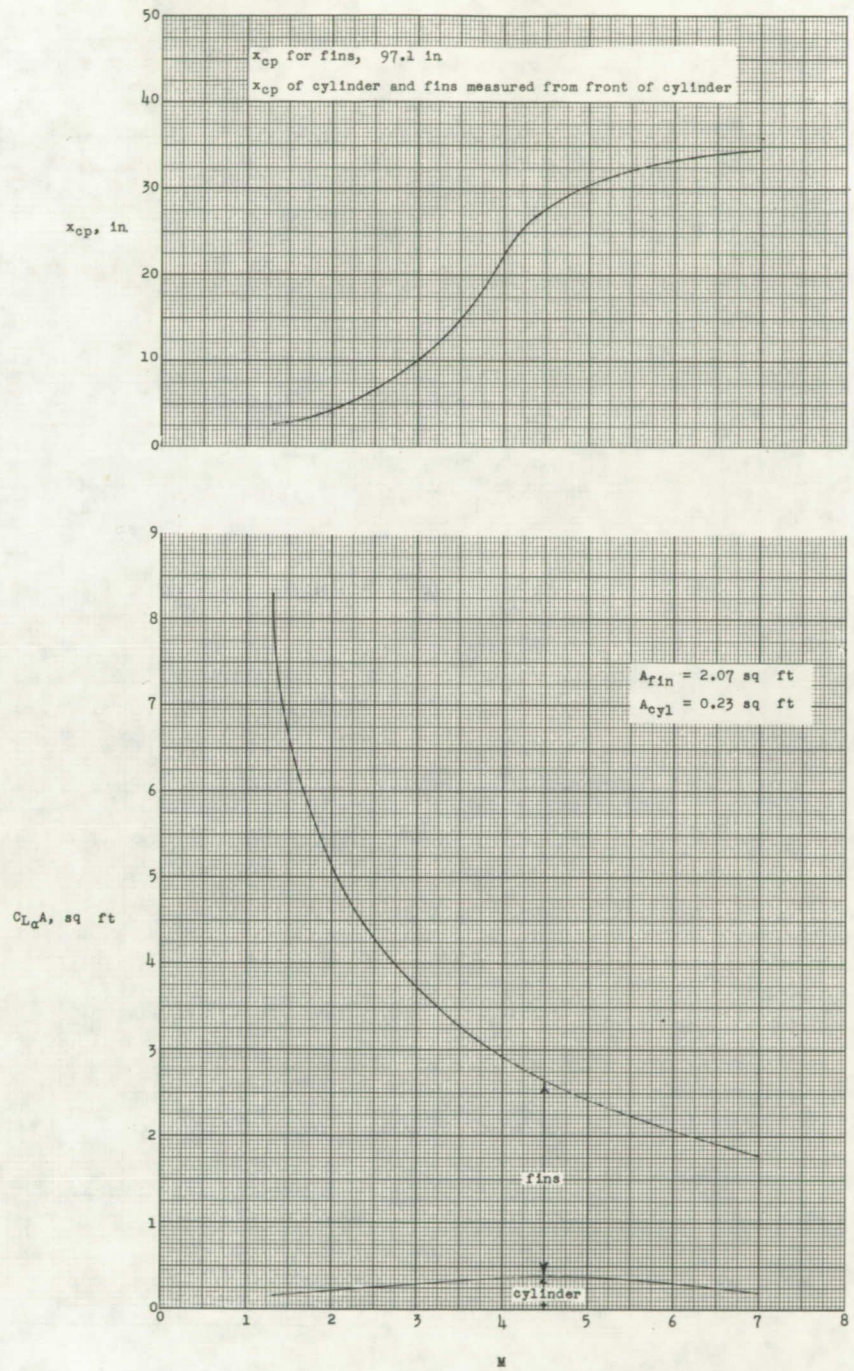

Figure 20.- Variation of the product of the calculated lift-curve slope and area with Mach number for the Cajun cylinder and fins and variation of the calculated center of pressure with Mach number for the Cajun cylinder.

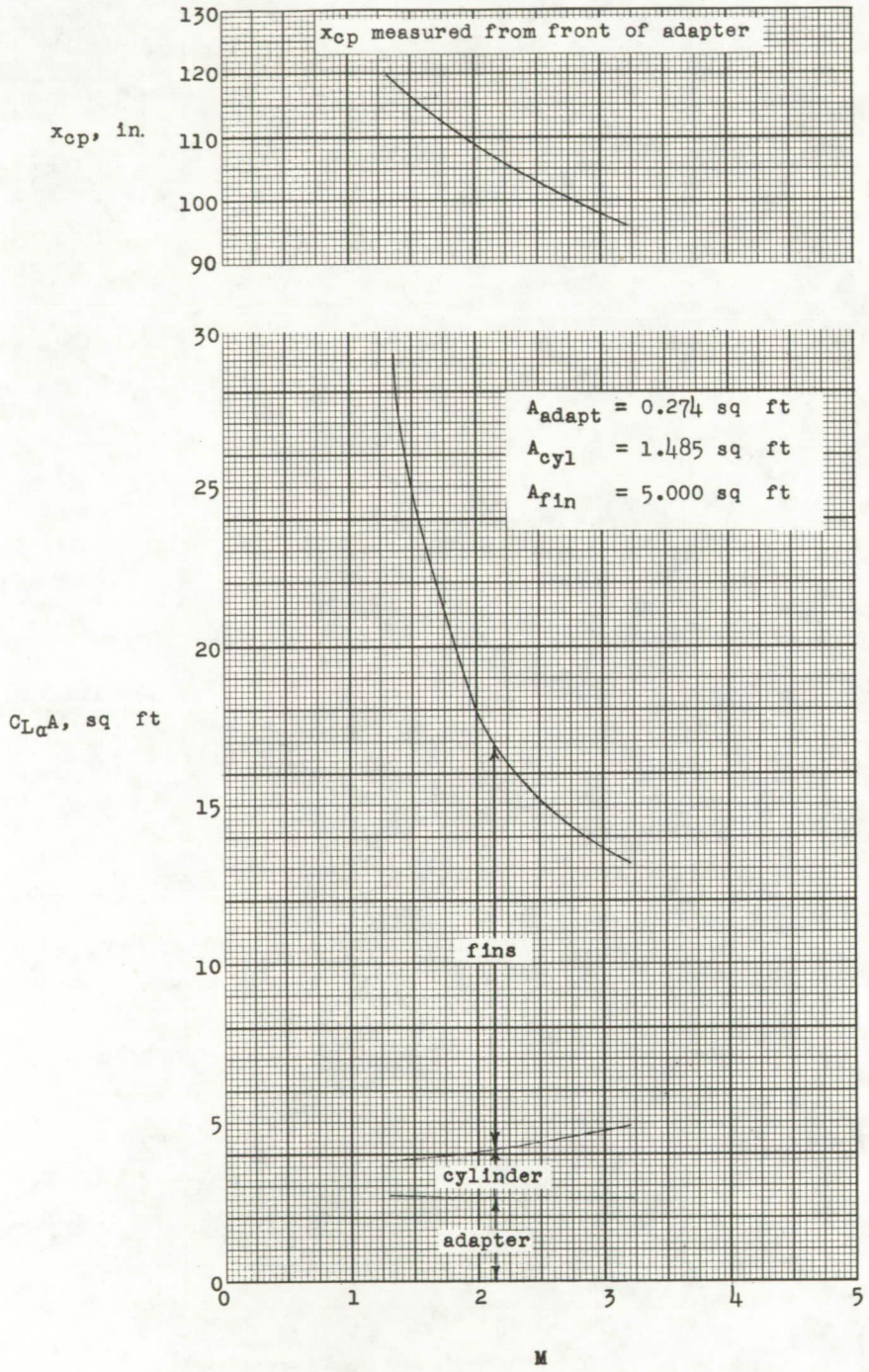

Figure 21.- Variation of the product of the calculated lift-curve slope and area and calculated center of pressure with Mach number for the Nike booster.

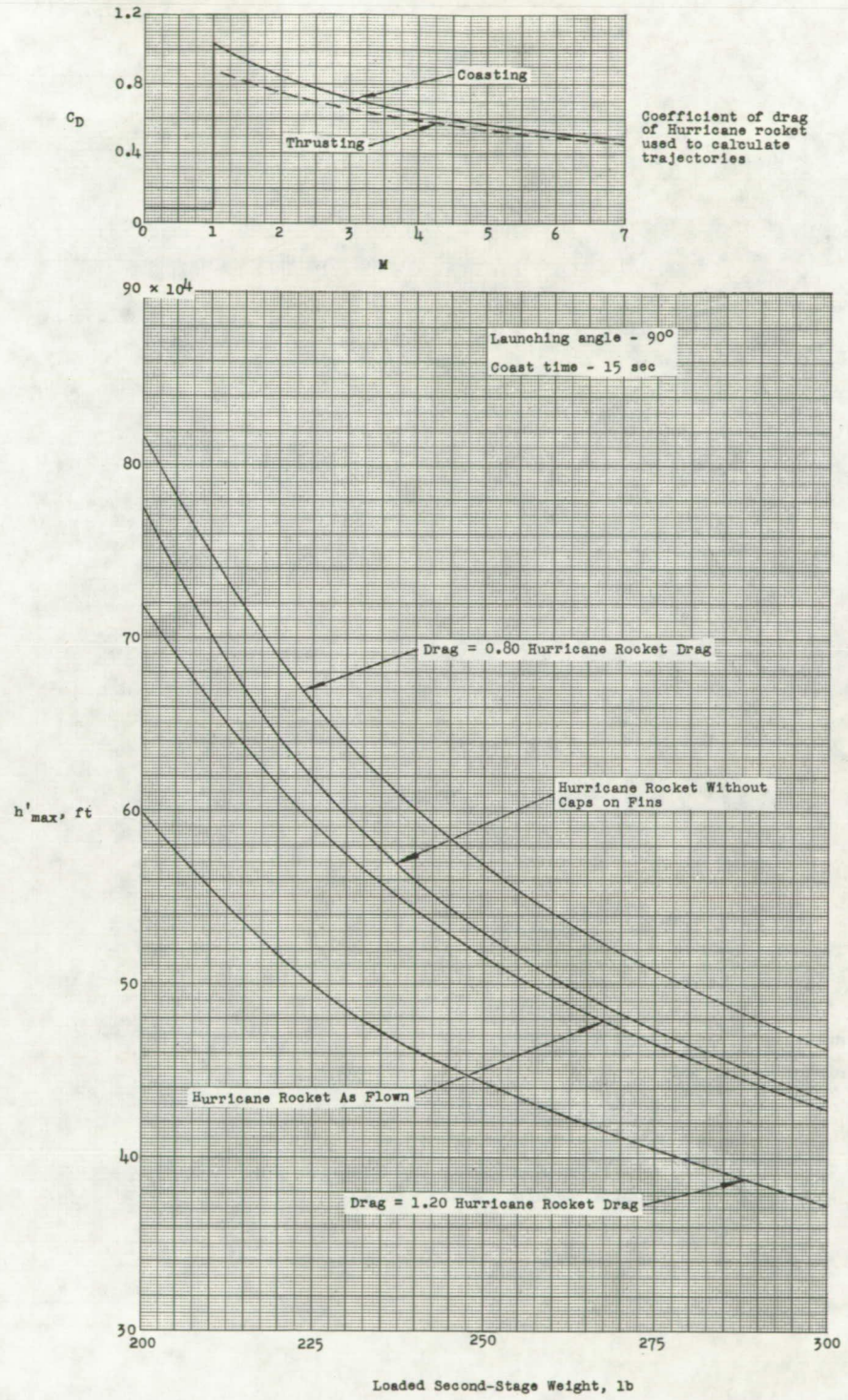

Figure 22.- Variation of calculated maximum altitude with loaded second-stage weight for a given drag condition.

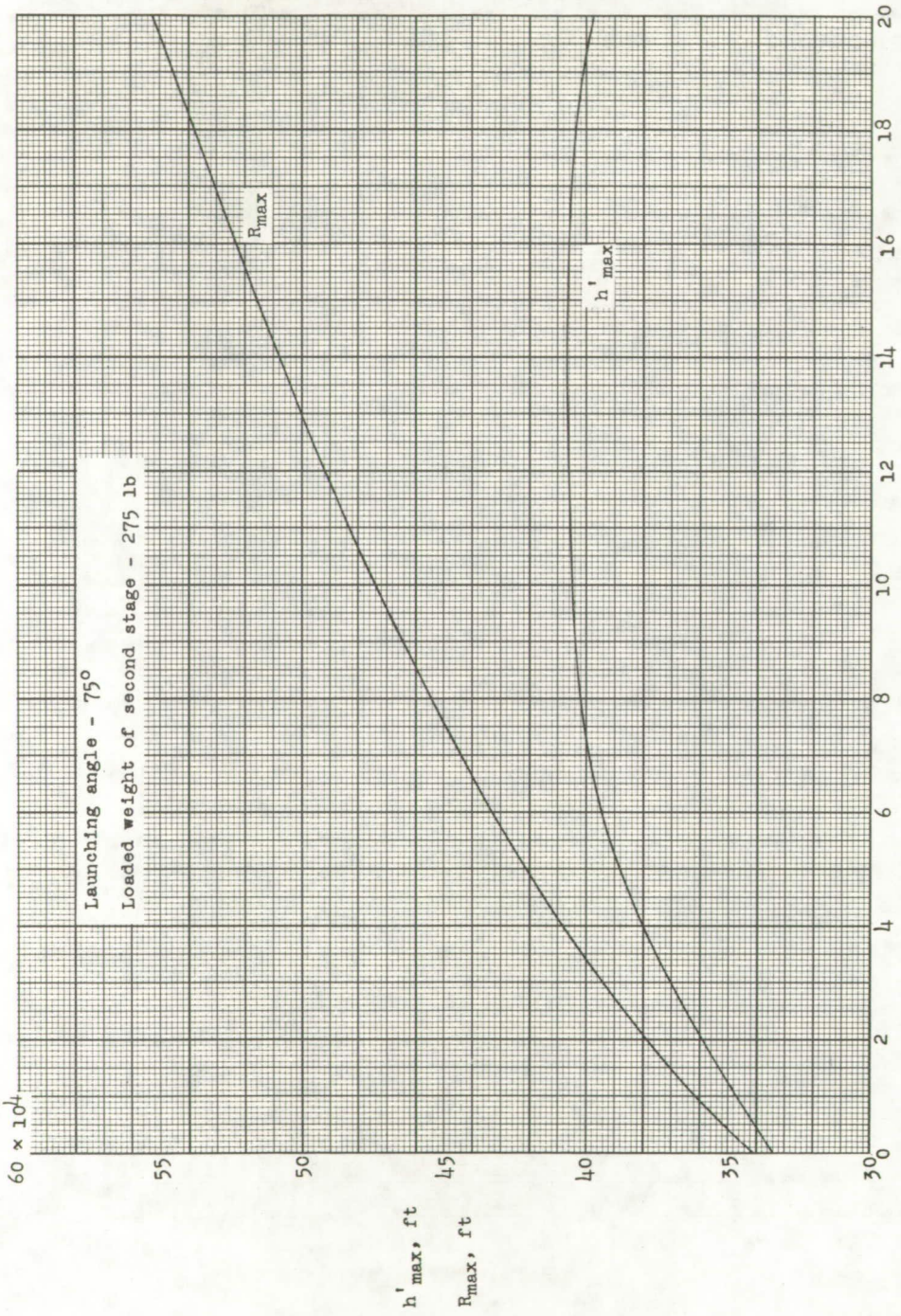

Figure 23.- Variation of calculated maximum altitude and calculated maximum range of the hurricane rocket with time between burnout of the first stage and firing of the second stage.

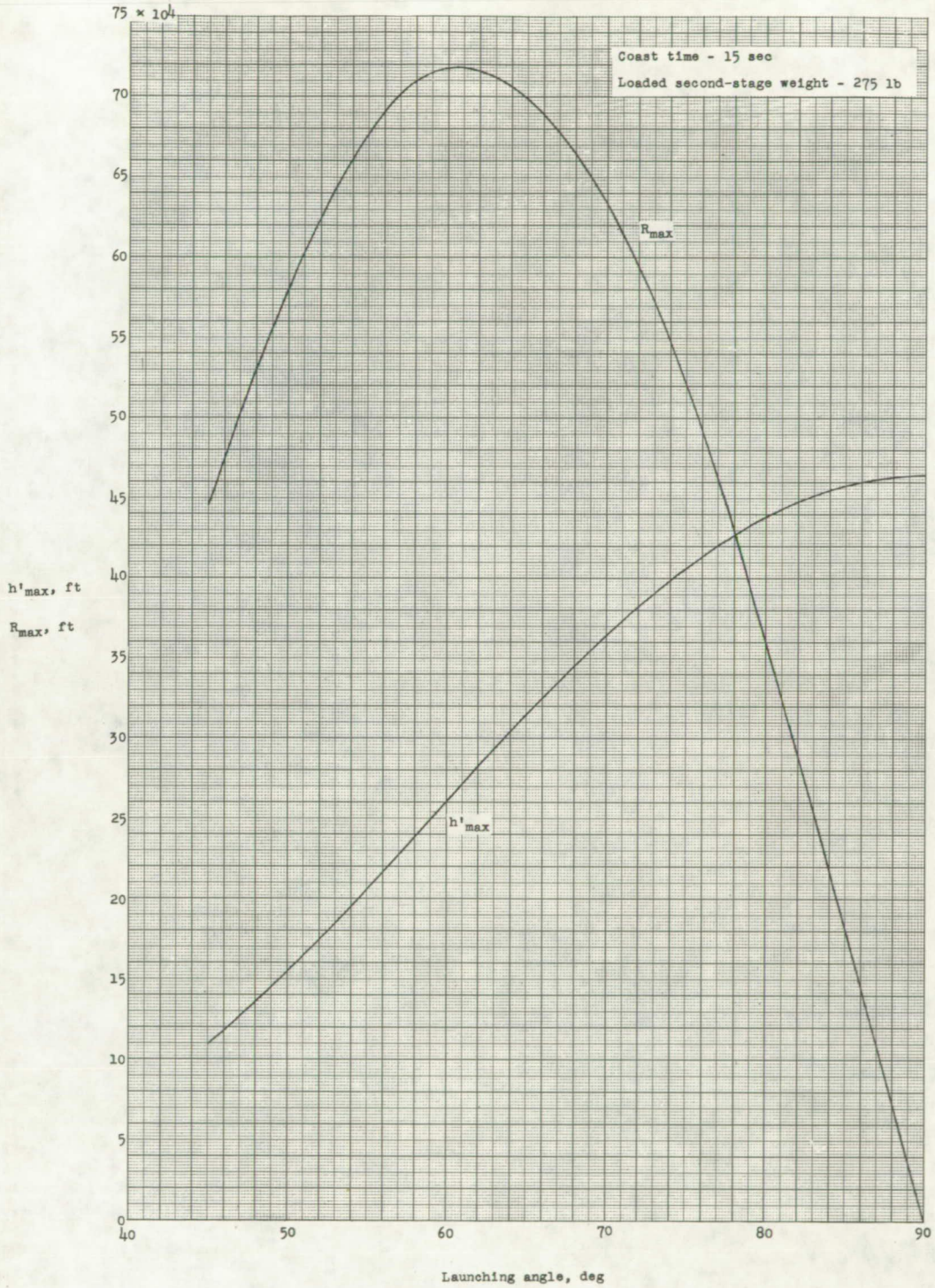

Figure 24.- Variation of calculated maximum altitude and calculated maximum range of the hurricane rocket with launching angle.